

Comparisons of land cover and LAI estimates derived from ETM+ and MODIS for four sites in North America: a quality assessment of 2000/2001 provisional MODIS products

Warren B. Cohen^{a,*}, Thomas K. Maier-sperger^b, Zhiqiang Yang^b, Stith T. Gower^c, David P. Turner^b, William D. Ritts^b, Mercedes Berterretche^{b,1}, Steven W. Running^d

^aForestry Sciences Laboratory, Pacific Northwest Research Station, USDA Forest Service, 3200 SW Jefferson Way, Corvallis, OR 97331, USA

^bForestry Sciences Laboratory 020, Department of Forest Science, Oregon State University, Richardson Hall, Corvallis, OR 97331-5752, USA

^cDepartment of Forest Ecology and Management, 1630 Linden Dr., University of Wisconsin, Madison, WI 53706, USA

^dSchool of Forestry, University of Montana, Missoula, MT 59812, USA

Received 12 February 2003; received in revised form 2 June 2003; accepted 6 June 2003

Abstract

The MODIS land science team produces a number of standard products, including land cover and leaf area index (LAI). Critical to the success of MODIS and other sensor products is an independent evaluation of product quality. In that context, we describe a study using field data and Landsat ETM+ to map land cover and LAI at four 49-km² sites in North America containing agricultural cropland (AGRO), prairie grassland (KONZ), boreal needleleaf forest, and temperate mixed forest. The purpose was to: (1) develop accurate maps of land cover, based on the MODIS IGBP (International Geosphere–Biosphere Programme) land cover classification scheme; (2) derive continuous surfaces of LAI that capture the mean and variability of the LAI field measurements; and (3) conduct initial MODIS validation exercises to assess the quality of early (i.e., provisional) MODIS products. ETM+ land cover maps varied in overall accuracy from 81% to 95%. The boreal forest was the most spatially complex, had the greatest number of classes, and the lowest accuracy. The intensive agricultural cropland had the simplest spatial structure, the least number of classes, and the highest overall accuracy. At each site, mapped LAI patterns generally followed patterns of land cover across the site. Predicted versus observed LAI indicated a high degree of correspondence between field-based measures and ETM+ predictions of LAI. Direct comparisons of ETM+ land cover maps with Collection 3 MODIS cover maps revealed several important distinctions and similarities. One obvious difference was associated with image/map resolution. ETM+ captured much of the spatial complexity of land cover at the sites. In contrast, the relatively coarse resolution of MODIS did not allow for that level of spatial detail. Over the extent of all sites, the greatest difference was an overprediction by MODIS of evergreen needleleaf forest cover at the boreal forest site, which consisted largely of open shrubland, woody savanna, and savanna. At the agricultural, temperate mixed forest, and prairie grassland sites, ETM+ and MODIS cover estimates were similar. Collection 3 MODIS-based LAI estimates were considerably higher (up to 4 m² m⁻²) than those based on ETM+ LAI at each site. There are numerous probable reasons for this, the most important being the algorithms' sensitivity to MODIS reflectance calibration, its use of a prelaunch AVHRR-based land cover map, and its apparent reliance on mainly red and near-IR reflectance. Samples of Collection 4 LAI products were examined and found to consist of significantly improved LAI predictions for KONZ, and to some extent for AGRO, but not for the other two sites. In this study, we demonstrate that MODIS reflectance data are highly correlated with LAI across three study sites, with relationships increasing in strength from 500 to 1000 m spatial resolution, when shortwave-infrared bands are included.

© 2003 Elsevier Inc. All rights reserved.

Keywords: Land cover; Leaf area index; ETM+; MODIS; BigFoot; IGBP; Validation

1. Introduction

Human impacts on the Earth system are considerable. Losses of native vegetation cover, biodiversity, and coastal ecosystems all threaten the functioning of the integrated processes that sustain life on Earth (Wilson & Peter, 1988). Burning of fossil fuels and large-scale conversion of prima-

* Corresponding author. Tel.: +1-541-750-7322; fax: +1-541-758-7760.

E-mail addresses: warren.cohen@orst.edu (W.B. Cohen), david.turner@oregonstate.edu (D.P. Turner).

¹ Current address: Ingenieros Consultores Asociados, 19 de abril 3482, Montevideo 11700, Uruguay.

ry forest to other uses and states are contributing to an increasing CO₂ concentration and probable accelerated changes in climate (IPCC, 2001). Pollution from various sources is degrading vast areas of land and volumes of ocean and atmosphere (NRC, 1999). As a result, there are now significant national and international efforts to develop a global biosphere monitoring system (Running et al., 1999; Townshend & Justice, 2002). A keystone component of that system is NASA's Earth Observation System (EOS) Terra satellite platform, launched in 1999. Perhaps the most important sensor on that platform for land surface observations is MODIS, the Moderate Resolution Imaging Spectroradiometer (Justice et al., 2002).

Associated with the Terra platform is a series of science teams devoted to producing useful products from the various sensors onboard the satellite. For the MODIS sensor, the land team produces a number of standard products, such as surface reflectance, land surface temperature, bidirectional reflectance distribution function and albedo, land cover and cover change, vegetation indices, thermal anomalies and fire, leaf area index (LAI) and fraction of photosynthetically active radiation absorbed (fAPAR), and net photosynthesis and net primary productivity (NPP) (Justice et al., 2002). Critical to the success of MODIS and other sensor products is an independent evaluation of product quality. For this purpose, a system of land validation core sites that represent a range of biome types where validation activities are concentrated has been established (Morisette, Privette, & Justice, 2002). At most of the sites, there is an existing program of long-term measurements and infrastructure to support in situ measurements that can be used to assess the quality of (or "validate") MODIS land data products.

For MODIS products related to the global carbon cycle, the most important validation core sites have a micrometeorological tower that uses eddy covariance methods to measure exchanges of CO₂, water vapor, and energy between terrestrial ecosystem and atmosphere (Running et al., 1999). These sites belong to a network known as FLUXNET, whose goals are to understand the mechanisms controlling fluxes across a spectrum of time and space scales (Baldocchi et al., 2001). Flux towers have a "footprint" over which measurements are made. Footprints vary in size, shape, and orientation depending on vegetation structure, height of tower above the vegetation, and wind speed and direction, but are generally considered to be about 1 km² in size. Although these are critical elements of a validation system for carbon-related MODIS products (Running et al., 1999), their size and the lack of detailed measurements of vegetation biophysical properties mean it is difficult to use them alone to directly validate MODIS products.

One project that is bridging the gap between tower measurements and MODIS is BigFoot (<http://www.fsl.orst.edu/larse/bigfoot/>) (Running et al., 1999). The BigFoot project is working at nine flux tower sites from Alaska to Brazil, each one representative of one or two distinct biomes, including the Arctic tundra; boreal evergreen needleleaf

forest; temperate cropland, grassland, evergreen needleleaf forest, and deciduous broadleaf forest; desert grassland and shrubland; and tropical evergreen broadleaf forest. BigFoot collects field-based data over 25 km² (5 × 5 km), and uses Landsat ETM+ image data and ecosystem process models to characterize 49 km² (7 × 7 km) around each tower. Our field sampling design is a nested spatial series to facilitate geostatistical analyses (Burrows et al., 2002). Field data are used both to develop site-specific algorithms for mapping and modeling land cover, LAI, fAPAR, and NPP, and to characterize the errors in derived surfaces of those variables. Direct comparisons of BigFoot- and MODIS-derived surfaces can help interpret possible sources of error in MODIS-derived surfaces and facilitate improvements to MODIS algorithms (Cohen & Justice, 1999; Morisette et al., 2002).

In this paper, we describe the methods used by BigFoot to map land cover and LAI at four sites, and present results in the context of MODIS validation. Specific objectives were to:

- develop accurate maps of land cover, based on the MODIS IGBP (International Geosphere–Biosphere Programme) land cover classification scheme;
- derive continuous surfaces of LAI that capture the mean and variability of the LAI field measurements; and
- conduct initial MODIS validation exercises to assess the quality of early (i.e., provisional) MODIS products.

2. Methods

2.1. Study sites

The four sites of this study include NOBS (Northern Old Black Spruce), HARV (Harvard Forest), KONZ (Konza Prairie), and AGRO (an agricultural system in Illinois). These sites were described in detail by Campbell, Burrows, Gower, and Cohen (1999) and through links accessible at <http://www.fsl.orst.edu/larse/bigfoot/>. NOBS is a boreal forest in northern Manitoba, Canada (Fig. 1), and was a site used in the Boreal Ecosystem Atmosphere Study (BOREAS, Sellers et al., 1997). The site is predominantly forested with black spruce stands of variable density, but contains numerous wetlands, small open water bodies, small aspen stands, extensive moss cover, and a large, recently burned area in the southern part of the study site. HARV is located in western Massachusetts and is predominantly a closed hardwood forest system with some small patches of conifer and mixed hardwood–conifer stands. Additionally, there are a few marshy lowland areas and rural residential development and pastures. KONZ is a tallgrass prairie in central Kansas and was the focus of the FIFE study in the 1980s (Sellers, Hall, Asrar, Strebel, & Murphy, 1992). In addition to grassland, there are areas of gallery forest and some croplands in the northern part of the study site. AGRO is a series of private farmlands containing annually alternating crops of

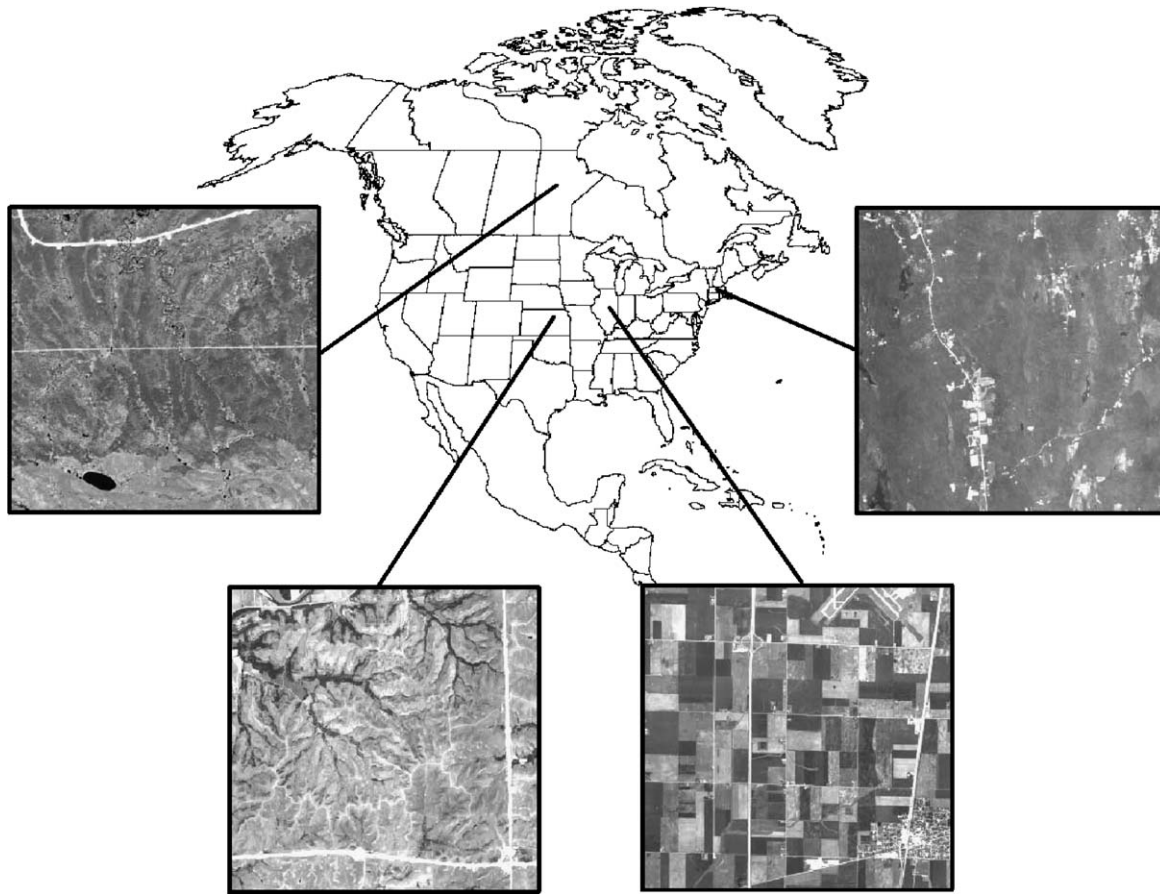


Fig. 1. Location of study sites in North America, and 1-m resolution panchromatic images of the 7×7 km sites. Clockwise from upper right: HARV, AGRO, KONZ, NOBS.

soybeans and corn. Numerous farmyards dot the landscape, and a rural community occupies the southeast corner of the site.

2.2. Sample design and field measurements

The sample design was a nested spatial series (Burrows et al., 2002) that permits explicit examination of spatial covariation among field-measured ecosystem properties using variograms and cross-variograms (Cressie, 1991). At each site, there were approximately 100, 25×25 m plots where land cover, LAI, fAPAR, and NPP were measured/observed at five to nine subplots per plot. Subplot measurements were averaged to provide a single value for each measured variable at each plot. Plot locations were determined using a real-time differential GPS. The accuracy of the system was <0.5 m in both the x and y dimensions (Burrows et al., 2002). Initial measurements were made in 2000, with remeasurements at some sites in 2001. At NOBS, LAI calculations were based on measurements from 1999.

At each site, LAI was measured at five subplots per plot using methods described by Gower, Kucharik, and Norman (1999) and Campbell et al. (1999). The methods included (at NOBS) allometric equations developed during BOREAS,

optical methods using a LAI-2000 (at HARV and KONZ), and standard, direct harvest methods (at AGRO). Optical measurements were corrected for clumping and the like, as described by Gower et al. (1999) and Burrows et al. (in review). Except at NOBS (where allometric equations based on diameter at breast height were used), measurements were made at several time periods during the growing season in 2000. At NOBS, percent tree cover was measured at nine systematically spaced subplots using an upward-looking digital camera. The imaged canopy projection area was dependent on tree height and the field of view of the camera, which was 30° . At approximately 10-m height, this means that among the nine subplots, nearly 100% of the canopy area in each plot was imaged. In the lab, each of the nine photos per plot was sampled using a grid of 99 points to derive the percent live tree canopy cover at each plot (Cohen, Maierpserger, Gower, & Tumer, 2003).

2.3. ETM+ imagery and preprocessing

Multidate ETM+ imagery was used at each site to develop the maps for 2000 (Table 1). At NOBS, two dates were used, one from the winter (which contrasts forest against a snow background) and the other from early-

Table 1
ETM+ images used for mapping at each site in 2000

Site	Path/row	Date
NOBS	34/21	13-Mar-00
	33/21	10-Jun-00
HARV	13/30	31-Aug-99
	12/31	13-Oct-00
	13/30	23-Dec-00
KONZ	28/33	7-Jun-00
	28/33	9-Jul-00
	28/33	25-Jul-00
	28/33	11-Sep-00
AGRO	22/32	26-Apr-00
	22/32	29-Jun-00
	22/32	15-Jul-00
	22/32	1-Sep-00

midgrowing season. At HARV, there was no cloud-free ETM+ image from the 2000 growing season. Thus, for this site, we used a growing season image from 1999 and two postgrowing season images from 2000. For KONZ and AGRO, imagery from four dates was used to capture the growing season from April (AGRO)/June (KONZ) through September. All imagery was georeferenced, radiometrically calibrated, and translated into Tasseled Cap brightness, greenness, and wetness. All images were acquired at level 1G processing, with a cell size of 30 m, and UTM (WGS84) projection. At NOBS, a panchromatic IKONOS image was registered to the Earth's surface using several GPS points collected in the field. The June image was then positionally shifted (i.e., offset in the x and y directions without resampling) to match the IKONOS image and the March image was shifted to match the June image. At the other three sites, the positional accuracy of the ETM+ image native map projection was judged by direct comparison with USGS digital orthophoto quadrangles (DOQs) at a 9×9 km area centered on the study site. After all imagery at these sites was positionally shifted to provide the best spatial match with the DOQs, the images were resampled to 25-m resolution, with <0.5 -pixel RMSE.

The COST absolute radiometric correction model of Chavez (1996) was applied to each image to convert digital counts to reflectance. Radiometrically “dark” objects were assumed to have 2% reflectance across all bands. For each site, the midgrowing season image was selected as a reference image and all other dates of imagery were relatively normalized to it, as a fine-tuning for multirate, interimage calibration. The method used was similar to that of Oetter, Cohen, Berterretche, Maiersperger, and Kennedy (2001) and of the Ridge Method of Kennedy and Cohen referred to by Song, Woodcock, Seto, Pax Lenney, and Gillespie (2001), which are an adaptation of standard band-by-band relative normalization procedures based on collocated bright and dark targets. As the COST model is not appropriate for low sun-angle situations, the March image from NOBS and the fall and winter images from HARV were converted to reflectance using a more basic dark-object-subtraction model. Further,

no relative normalization was performed for the NOBS dataset, due to major spectral property differences between the two dates, given the backdrop of ice and snow for the March scene and of vegetation and water for the June scene (Cohen et al., 2003).

No published transformation exists to convert atmospherically corrected ETM+ spectral data to Tasseled Cap indices. However, Crist (1985) derived coefficients for brightness, greenness, and wetness from ground-based spectral data that can be applied to Landsat reflectance factor data. Slight differences in spectral band width and position, as well as calibration, exist between Landsat TM and ETM+ (Teillet et al., 2001; Vogelmann et al., 2001), but they are similar enough to assume that the differences in Tasseled Cap indices derived for data from the two different sensors are small. We tested this assumption using TM and ETM+ images acquired within a few days of each other (Path 46/Row 29) over western Oregon in 1999. First, we converted atmospherically corrected TM DN data to the Tasseled Cap indices using the coefficients in Crist and Cicone (1984). We then converted the atmospherically corrected TM DN data to reflectance using published coefficients and formulae, before using the Crist (1985) coefficients to convert the reflectance data to Tasseled Cap indices. Finally, we atmospherically corrected the ETM+ data and then converted the reflectance data to the Tasseled Cap indices using the Crist (1985) coefficients. A comparison of the brightness, greenness, and wetness images from the three methods showed that they were highly intercorrelated at a level of roughly 95%. We then transformed each individual image used in this study into brightness, greenness, and wetness indices.

2.4. Land cover mapping

MODIS land cover products (MOD12Q1) exist in several variants (Morissette et al., 2002). For BigFoot, we mapped to the IGBP variant, which has 17 cover classes (Table 2). At AGRO, a modifier was added to account for ecologically significant differences between corn (Class 12a) and soybeans (Class 12b) within Class 12 (croplands). BigFoot land cover mapping was based on the multirate stack of ETM+ band data or Tasseled Cap indices at each site. The goal was to map land cover at the peak of the growing season for 2000. First, an unsupervised classification was conducted to stratify Classes 0 (water), 13 (urban/built), and 16 (barren) from vegetated classes. There were no events of Classes 2 (evergreen broadleaf forest), 3 (deciduous needleleaf forest), 14 (cropland/natural vegetation mosaic), or 15 (snow/ice). Class 11 (permanent wetland) is defined by the presence of water rather than by vegetation (or spectral) characteristics (Table 2). Thus, the only way to accurately map this class was to hand digitize occurrences of it, where growing season standing water was evident. This class existed only at NOBS and HARV. Specific methods of analysis for the remaining vegetated classes varied by site.

Table 2
MOD12Q1, IGBP land cover classes

Broad cover type	Class number	Class name	Class description
Natural vegetation	1	Evergreen needleleaf forest	Lands dominated by woody vegetation with a percent cover >60% and height exceeding 2 m. Almost all trees remain green all year. Canopy is never without green foliage.
	2	Evergreen broadleaf forest	Lands dominated by woody vegetation with a percent cover >60% and height exceeding 2 m. Almost all trees and shrubs remain green year round. Canopy is never without green foliage.
	3	Deciduous needleleaf forest	Lands dominated by woody vegetation with a percent cover >60% and height exceeding 2 m. Consists of seasonal needleleaf tree communities with an annual cycle of leaf-on and leaf-off periods.
	4	Deciduous broadleaf forest	Lands dominated by woody vegetation with a percent cover >60% and height exceeding 2 m. Consists of broadleaf tree communities with an annual cycle of leaf-on and leaf-off periods.
	5	Mixed forest	Lands dominated by trees with a percent cover >60% and height exceeding 2 m. Consists of tree communities with interspersed mixtures or mosaics of the other four forest types. None of the forest types exceeds 60% of landscape.
	6	Closed shrubland	Lands with woody vegetation less than 2-m tall and with shrub canopy cover >60%. The shrub foliage can be either evergreen or deciduous.
	7	Open shrubland	Lands with woody vegetation less than 2 m tall and with shrub canopy cover between 10% and 60%. The shrub foliage can be either evergreen or deciduous.
	8	Woody savanna	Lands with herbaceous and other understory systems, and with forest canopy cover between 30% and 60%. The forest cover height exceeds 2 m.
	9	Savanna	Lands with herbaceous and other understory systems, and with forest canopy cover between 10% and 30%. The forest cover height exceeds 2 m.
	10	Grasslands	Lands with herbaceous types of cover. Tree and shrub cover is less than 10%.
	11	Permanent wetlands	Lands with a permanent mixture of water and herbaceous or woody vegetation. The vegetation can be present in either salt, brackish, or fresh water.
Developed and mosaic lands	12	Cropland	Lands covered with temporary crops followed by harvest and a bare soil period mosaic lands (e.g., single and multiple cropping systems). Note that perennial woody crops will be classified as the appropriate forest or shrub land cover type.
	13	Urban/Built	Land covered by buildings and other man-made structures.
	14	Cropland/natural vegetation mosaic	Lands with a mosaic of croplands, forests, shrubland, and grasslands in which no one component comprises more than 60% of the landscape.
Nonvegetated lands	15	Snow/ice	Lands under snow/ice cover throughout the year.
	16	Barren	Lands with exposed soil, sand, rocks, or snow and never has more than 10% vegetated cover during any time of the year.
	0	Water	Oceans, seas, lakes, reservoirs, and rivers. Can be either fresh or salt-water bodies.

2.4.1. NOBS 2000

At NOBS, most of the vegetation could be characterized along a percent tree cover gradient. Thus, at this site, we modeled live tree cover directly using reduced major axis regression (RMA), as described by Cohen et al. (2003). Using the resultant predicted surface of continuous tree cover percentages, we labeled individual pixels as Class 9 (savanna, 10–30%), Class 8 (woody savanna, 30–60%), Class 1 (evergreen needleleaf forest, >60%), or as unclassified. We then compared a map of this interim classification with the 4-m multispectral IKONOS image from Fig. 1 and color-infrared airphotos acquired during 1999. In this landscape, Class 4 (deciduous broadleaf forest) existed in small patches that were easily distinguished on the reference IKONOS and airphoto imagery. Thus, using these reference data, we hand digitized around Class 4 patches that were originally designated as Class 1 using the percent tree cover layer, and

re-labeled these as Class 4. Remaining unclassified pixels were labeled as either Class 6 (closed shrubland) or Class 7 (open shrubland).

2.4.2. HARV 2000

At HARV, most of the vegetation consisted of gradients of percent tree cover and hardwood to conifer composition, a problem well suited to mixture modeling (Smith, Ustin, Adams, & Gillespie, 1990). For this, the August 31 ETM+ band reflectance data were transformed into unstandardized principal components (PCs). A bivariate plot of the first two PC axes formed a triangle. The PC image was clustered ($n = 100$) and clusters plotted into PC space to find endmembers (vertices of the aforementioned triangle). Clusters of pixels at the three vertices corresponded to pure grass, conifer, and hardwood in the image. These endmember samples had some spectral variability, but were well defined

spatially within the image domain. Using these endmembers, constrained linear unmixing was performed on the six-band ETM+ Aug. 31, 1999, image using commonly available software. Fraction images were then combined into the MOD12Q1, IGBP ruleset to form grassland (Class 10), savanna, woody savanna, evergreen needleleaf forest, deciduous broadleaf forest, and mixed forest (Class 5). Mixture-modeled classes were nested within the original unsupervised classification to produce the final land cover map. All class labeling and related site knowledge were based on ADAR (<http://www.possys.com/index.htm>) image interpretation, field notes, ground photography, and color-IR photography acquired during summer, 2000.

2.4.3. KONZ 2000

The KONZ site is largely a grassland biome, containing significant amount of grass and woody vegetation in both shrub and tree form. At the grain of ETM+ data, there was little or no unvegetated ground cover except for barren areas associated with roads and the like. Trees and shrubs were essentially indistinguishable using the ETM+ data; however, they were well-defined spatially at the site. These and subsequent land cover calls were made using 2000 ADAR imagery and airphotos, and notes and hand-held photos from site visits in 2000. In a fashion similar to NOBS, where a tree cover regression model was developed, at KONZ, an RMA model for woody cover was developed using the four-date Tasseled Cap image stack. To accomplish this, we randomly distributed 100 1-ha plots within the broad vegetated class stratified by the preliminary unsupervised classification. Plots were required to be at least 200 m apart, based on the range of a semivariogram of the June greenness image. For each plot, we interpreted the percent cover of woody vegetation, grass, and barren (essentially nonexistent at each plot). The woody cover model was applied to the appropriate ETM+ pixels, which were then labeled as follows: grassland (<10% woody cover), open shrubland (10–30% woody cover), woody savanna (30–60% woody cover), and deciduous broadleaf forest (>60% woody cover). This method of label assignment precluded labels for savanna and closed shrubland. Although these existed at the site in rare, small patches at the grain size of ETM+, it captured the dominant vegetation patterns very well. Following these assignments, hand editing was used to minimize confusion between grassland, open shrubland, and woody savanna, and to isolate and label croplands (which existed in the northwestern part of the site).

2.4.4. AGRO 2000

At AGRO, unsupervised classification of the Tasseled Cap multivariate stack was used to distinguish croplands from all other types, including isolated patches of grassland located around an airport runway and at an interstate “cloverleaf”. Two types of cropland were distinguished: corn and soybeans. All labels were derived from plot observations, ADAR imagery, and airphotos acquired in

2000. Hand-editing was used to recode minor mislabeling within specific fields, and to identify roads and water canals.

2.4.5. 2000 error characterization

Characterization of land cover mapping errors was based on an independent sample 1-ha plots at each site, except AGRO. Samples were selected by stratified random sampling, where the strata were land cover classes and the placement of individual plots next to other plots was never closer than the range of the semivariogram constructed from midgrowing season greenness (calculated from ETM+ data). Distribution of plots was weighted by land cover proportion, and the number of plots was variable by site (depending on site complexity). Observed land cover for these plots was determined from IKONOS and ADAR imagery. For AGRO, every crop field was visited during the growing season. ADAR was used to assess errors in the noncrop classes.

2.4.6. 2001 cover map updates

As the MODIS algorithms continue to be improved, it is important to continue examining the products derived from them. For NOBS, HARV, and KONZ, we updated the cover maps to 2001 for this purpose. Updates were accomplished by closely examining the ETM+ imagery from 2001 in relation to the 2000 land cover maps, 2001 airphotos, and other high spatial resolution imagery. As these sites are relatively stable from year to year (and as the size of each mapped area was small: 49 km²), we could easily identify areas that had changed due to minor disturbance processes. The changed areas (totaling 0.27%, 0.77%, and 0.00% of site area for NOBS, HARV, and KONZ, respectively), once identified, were relabeled within the 2000 maps to develop updated, 2001 land cover maps. AGRO is highly dynamic from year to year and we did not visit this site in 2001, thus the change detection procedure could not be done confidently.

2.5. LAI modeling and mapping

We used a regression approach to model LAI at each site for 2000. Regression analysis has been a popular empirical method of modeling the relationship between spectral data and LAI (Butera, 1986; Chen & Cihlar, 1996; Fassnacht, Gower, MacKenzie, Nordheim, & Lillesand, 1997; Turner, Cohen, Kennedy, Fassnacht, & Briggs, 1999). However, traditional (i.e., ordinary least squares, OLS) methods of regression are not sufficient when resulting biophysical surfaces derived from remote sensing are subsequently used to drive ecosystem process models, as is the case in the BigFoot project. With OLS regression, the variance of the predictions is commonly compressed relative to the variance of the observations (Curran & Hay, 1986). In BigFoot, to estimate NPP, we use mechanistic models that have nonlinear functions dependent on LAI. As such, compression of variance in LAI introduces error in the mechanistically modeled outputs. The degree of compression (and its

concomitant effect on NPP estimates) is a function of the correlation between the spectral data and the biophysical variable; low correlation, much compression, and vice versa.

In this study, the orthogonal RMA (Reduced Major Axis) regression method was used. We recently demonstrated the value of RMA relative to OLS regression to predict both tree cover at NOBS and LAI at AGRO (Cohen et al., 2003). To the extent possible, we developed separate models for each major vegetation cover class or class group. Two conditions had to be met for this stratification to be applied. First, there had to be enough plots in the class to develop a model (in this study, the number of plots per cover type ranged from 9 to 82, with a mean of 37; Table 3). Second, there had to be some meaningful predictive power to the model. Most regression analyses in remote sensing rely on a single spectral vegetation index (SVI) based on red and near-infrared reflectance from a single date of imagery (Tucker, 1979; Huete, Jackson, & Post, 1985; Sellers, 1987; Turner et al., 1999). There are compelling reasons for utilizing greater spectral dimensionality, and for including SVIs from multiple dates in a regression analysis. Here, we used multivariate brightness, greenness, and wetness to predict LAI. When including multiple SVIs and/or dates, it is useful to integrate these into a single index for regression modeling, particularly for RMA regression. For this, we employed canonical correlation analysis (CCA), which had the added benefit of aligning the spectral data with the variable of interest (Cohen et al., 2003), in this case LAI.

With both OLS and RMA regression done in a multiple SVI context, predictor variables (i.e., SVIs) must be selected based on their statistical significance (e.g., at a p value of 0.05). For each LAI model, we used forward stepwise regression. In each case, brightness, greenness, and wetness from all dates of available imagery were used as potential variables for a model. Prior to conducting stepwise regression, bivariate plots of all potential SVIs against LAI were evaluated to determine if transformations were required to

Table 4
LAI “fill” values for unsampled, and thus unmodeled, classes

Site	Value	Class	Percent of site area
NOBS	0.0	Water	2.2
	0.0	Barren	0.8
	0.0	Urban/built	1.2
HARV	0.0	Water	1.8
	0.0	Urban/built	0.6
	1.0	Grassland	4.5
	1.0	Permanent wetland	3.6
	1.5	Savanna	0.3
	2.0	Woody savanna	1.6
KONZ	0.0	Water	0.1
	0.0	Urban/built	2.9
	3.0	Cropland	4.3
	5.0	Deciduous broadleaf forest	7.2
AGRO	0.0	Water	0.7
	0.0	Urban/built	13.1
	1.0	Grassland	1.8

linearize relationships. Where necessary, standard log and square root transformations were used.

To map LAI across a study site, each model developed for a given class at a given site was applied to the relevant CCA axis and vegetation class from the land cover map. Some vegetation classes existed as small, scattered patches at a given site, e.g., the grassland class at AGRO. As we did not sample that class in the field, we used LAI values from the literature for these classes (Table 4).

2.5.1. 2000 LAI error characterization

Field-based LAI data are expensive to collect and process, so using them prudently is essential. There is a tradeoff between using all available observations to develop a regression model and having no independent observations to test the model, versus excluding a predetermined number of observations to test the model, but having a less robust model because it was developed on fewer points. The statistical literature provides several alternative, but related

Table 3
LAI models by site and cover class or class group

Site	Cover class/group	n	Correlation	Slope	Intercept	Spectral variables used ^a
NOBS	1	12	0.68	−38.8	127.9	610b
	8	57	0.66	1.4	4.3	313b, 610bg
	9	25	0.82	1.3	3.1	313bw, 610b
	4, 7, 11	9	0.68	1.7	4.2	313w
HARV	1	18	0.75	−0.6	5.0	831g, 1013bg, 1223bgw
	4	42	0.75	0.7	4.9	831bw, 1013bgw, 1223bg
	5	13	0.90	0.6	5.2	831bg, 1013g, 1223g
KONZ	10	82	0.54	0.5	1.9	607bgw, 709bgw, 725gw
	7, 8	17	0.58	0.9	2.3	607b, 709g, 725w, 911gw
AGRO	12 (a. soy only)	62	0.76	0.6	1.5	426bgw, 629bgw, 715bgw, 901bgw
	12 (b. corn only)	29	0.78	0.8	4.4	426bgw, 629bgw, 715bgw, 901bgw

See Table 2 for names associated with class numbers.

^a Variables are given by date (e.g., 610 equals June 10) and Tasseled Cap index (b is brightness, g is greenness, and w is wetness); the slope and intercept terms are for the CCA axis used for each model.

ways to address this problem: cross-validation, bootstrapping, and jackknifing (Efron & Gong, 1983). We used the cross-validation procedure that provides a nearly unbiased estimator of prediction error (Efron & Gong, 1983). This required, for each dataset and regression variant, that (where, e.g., $n=100$) 100 separate models be developed, each time with data from 99 observations. Then, each model was used to predict the observation that was left out, thus providing the predictions for all 100 plot observations that were needed to compare against the observed values (Cohen et al., 2003).

Additionally, predicted versus observed plots were developed and overall bias and variance ratios were calculated. Bias was calculated as the mean of the predicted values minus the mean of the observed values, such that a positive bias equated to a mean overprediction, and vice versa. Variance ratio was calculated as the standard deviation of the predicted values divided by the standard deviation of the observed values. As such, a ratio of greater than one meant that the prediction standard deviation was greater than the observed standard deviation, and vice versa.

2.5.2. 2001 LAI map updates

The NOBS 2000 BigFoot LAI surface was based on regression equations. To derive a 2001 LAI map, we updated the 2000 LAI map by applying the class-specific equations in Table 3 to pixels identified earlier as changed. In this case, we used the new labels to determine which model to use, but the models were applied to the 2001 ETM+ data. For areas that had not changed, we used the original LAI estimates. For HARV and KONZ, we had new field measurements, and these were used in conjunction with 2001 imagery and the 2001 land cover maps to develop 2001 LAI maps using a new set of models developed in the same way as those from 2000.

2.6. Comparisons with MODIS products

MODIS V003 (also known as Collection 3) provisional data are in the Integerized Sinusoidal Projection (ISIN, Seong, Mulcahy, & User, 2002) and BigFoot data are in

UTM WGS84. To compare MODIS and BigFoot products, we used the MODIS Reprojection Tool (<http://edc.usgs.gov/programs/sddm/modisdist/index.shtml>) to reproject BigFoot maps into ISIN (Fig. 2). This permitted direct overlay of land cover and LAI data products from MODIS and BigFoot. Although we can expect modest errors of coregistration (MODIS data have an expected registration error of <50 m at nadir; Wolfe et al., 2002), overlay in this way provided confidence in making direct spatial comparisons at the site level.

For land cover comparisons, MOD12Q1 Collection 3 products from 2000 were used (Friedl et al., 2002). At each site, we summarized these maps to characterize proportions of land cover classes and compared those with 2000 BigFoot products as frequency histograms. The 2001 MODIS MOD12Q1 Collection 3 product was likewise compared to the 2001 BigFoot products at NOBS, HARV, and KONZ.

Collection 3 MOD15A2 LAI products were not available for 2000 (<http://edcdaac.usgs.gov/modis/dataproduct.html>); for that year, only products based on poorly calibrated Collection 1 MODIS data were available. Thus, we used Collection 3 data from 2001 for our comparisons with both 2000 and 2001 BigFoot LAI maps. For this, we plotted the mean and standard deviation of MODIS LAI 8-day composite data for the year 2001 for the four sites. On the same graphs, mean and standard deviation of the 2000 and 2001 BigFoot ETM+ surfaces were plotted.

Subsequent to completing these analyses, some provisional V004 (i.e., Collection 4) LAI data started becoming available. Thus, we downloaded a small amount of those data for comparison with Collection 3 data to determine how they were different. Collection 4 data include certain improvements that are purported to be of better quality than Collection 3 products (http://modis-land.gsfc.nasa.gov/news/iniv_nws_pgs/c4_descrip.asp). For LAI, these include upstream data improvements such as better reflectance calibration. In addition, the LAI algorithm used an improved MODIS land cover map, and improved lookup tables for the main and backup algorithms. The latter improvement purportedly increased the number of high-quality retrievals

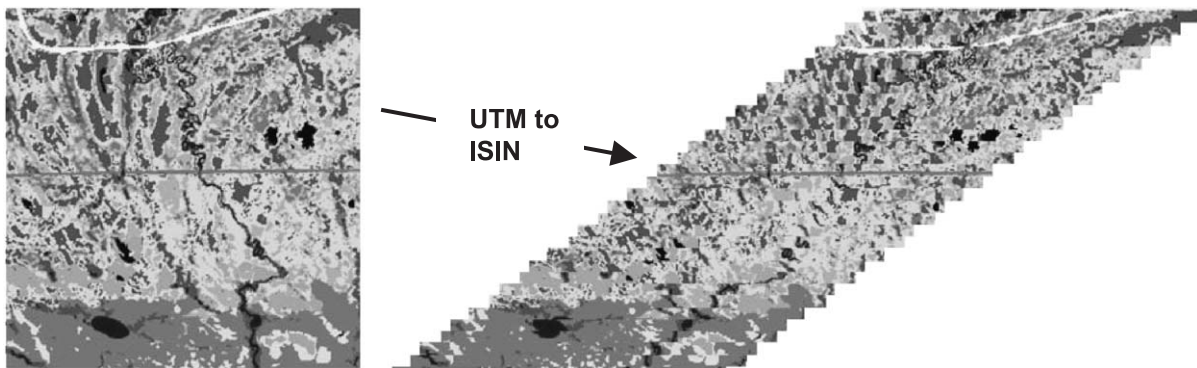


Fig. 2. Example of using the MODIS Reprojection Tool to translate the NOBS land cover map (based on ETM+) projected in UTM coordinates to the ISIN projection.

by 10%, removing a noted nonphysical peak in global LAI and improved agreement with ground measurements. The data we evaluated were for the period from July 4 through August 12, 2001, representing five 8-day composite bins for each 7×7 km site.

2.7. MODIS reflectance and LAI

When comparing BigFoot and MODIS Collection 3 LAI products, we noted significant discrepancies in the estimated values. This led us toward more close examination of the

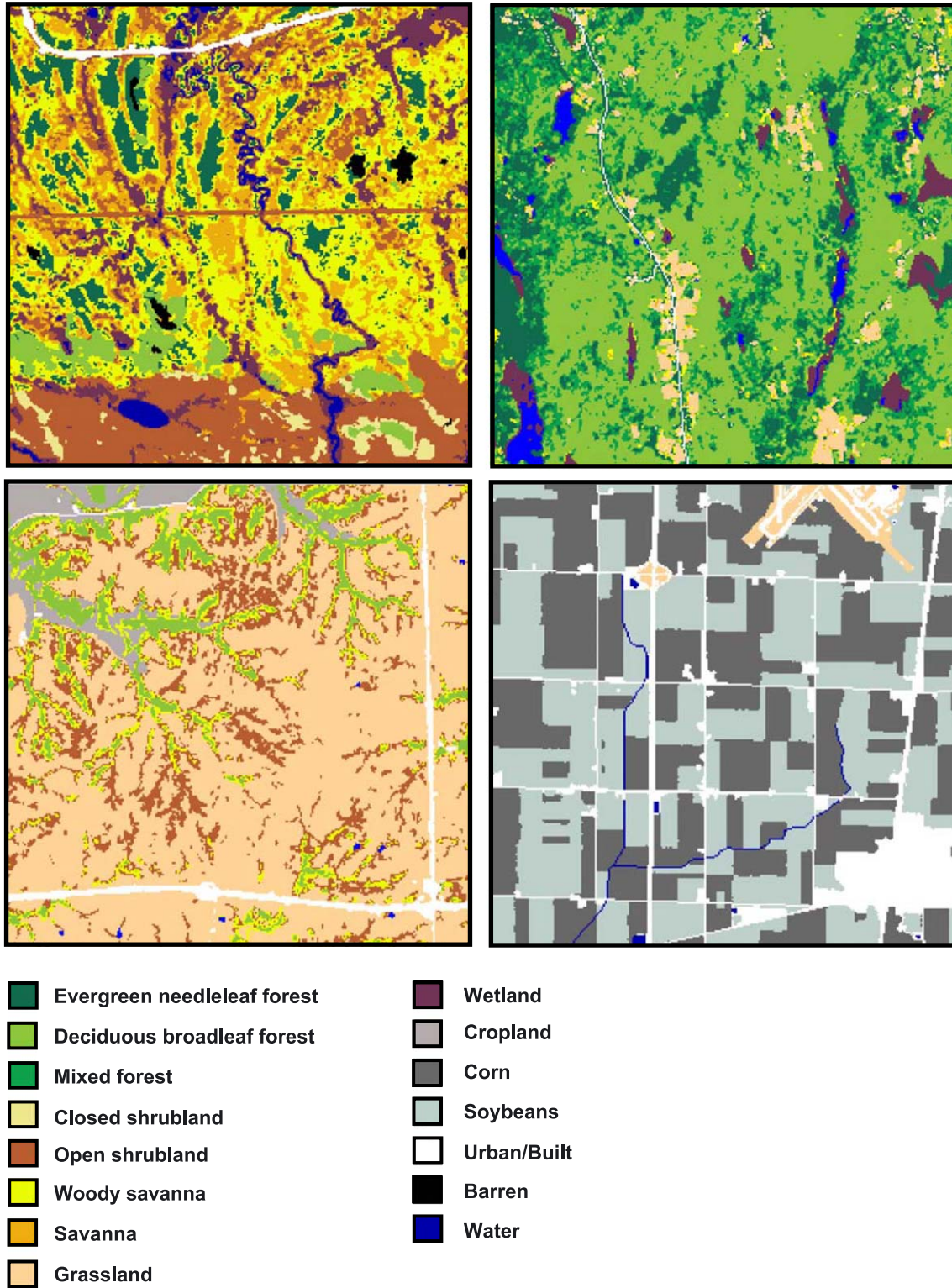


Fig. 3. BigFoot land cover maps based on ETM+ data for the four study sites (upper left, NOBS; upper right, HARV; lower left, KONZ; lower right, AGRO).

MOD15A2 algorithm, and consequently, the MODIS reflectance data in relation to LAI. The MODIS Collection 3 product was not based on a full implementation of the MOD15A2 algorithm; it uses a prelaunch land cover product based on AVHRR, and apparently relies almost exclusively on the use of red and near-infrared reflectance (akin to the NDVI) rather than reflectance from all MODIS bands. We first examined the relationships for NOBS, HARV, and KONZ between field-measured LAI and ETM+ NDVI.

These were compared with the relationships of LAI and new CCA axes developed for use across cover classes so the results would be consistent with those of the NDVI. Second, we repeated that exercise using MOD09GHK (the daily 500-m surface reflectance product) acquired close to growing season maximum LAI for the same sites in 2000 (August 24 for NOBS, July 20 for HARV, and August 24 for KONZ). LAI in this case was derived using a 500-m grid overlain on the ETM+ LAI surfaces that were spatially

Table 5
Error matrix for BigFoot 2000 land cover maps

Predicted Class	Site	Observed Class															
		Evergreen Needleleaf Forest	Deciduous Broadleaf Forest	Mixed Forest	Closed Shrubland	Open Shrubland	Woody Savanna	Savanna	Grassland	Permanent Wetland	Cropland	Corn	Soy	Urban/Built	Barren	Water	
Evergreen Needleleaf Forest	NOBS	21					11										
	HARV	16															
	KONZ																
	AGRO																
Deciduous Broadleaf Forest	NOBS		11														
	HARV		52	1													
	KONZ		14														
	AGRO																
Mixed Forest	NOBS																
	HARV	1	8	12			1										
	KONZ																
	AGRO																
Closed Shrubland	NOBS				6												
	HARV																
	KONZ																
	AGRO																
Open Shrubland	NOBS			1		21		2		1							
	HARV																
	KONZ					45	1	4	3								
	AGRO																
Woody Savanna	NOBS	1	1				50	8									
	HARV						1										
	KONZ			1			8	2									
	AGRO									2							
Savanna	NOBS						7	37	1								
	HARV							1									
	KONZ																
	AGRO																
Grassland	NOBS																
	HARV																
	KONZ					10			2	90							
	AGRO																
Permanent Wetland	NOBS					2				15							1
	HARV									3							
	KONZ																
	AGRO																
Cropland	NOBS																
	HARV																
	KONZ										9						
	AGRO																
Corn	AGRO											63					1
	AGRO											2	75	3			
Urban/Built	NOBS																
	HARV																
	KONZ																
	AGRO													8			
Barren	NOBS																8
	HARV																
	KONZ																
	AGRO																
Water	NOBS									1							7
	HARV																
	KONZ																
	AGRO																
Percent Correct	NOBS	0.95	0.92	0.86	0.86	0.91		0.74	0.76	0.67	0.79				1.00	0.88	0.81
	HARV	0.94	0.87	0.86			0.74	0.76	0.67	1.00							0.87
	KONZ		1.00				0.50	1.00	0.97		1.00						0.89
	AGRO						0.80	0.00				0.94	1.00	0.86	0.50	1.00	0.95
	All sites	0.95	0.90	0.86	0.86	0.84	0.74	0.68	0.96	0.82	1.00	0.94	1.00	0.90	0.90	0.91	0.88

registered to the MODIS data to calculate mean site-level ETM+ LAI estimates at a grain of 500 m. Finally, both datasets were spatially aggregated to 1000 m and compared once again.

3. Results

3.1. BigFoot land cover

The BigFoot land cover maps (Fig. 3) varied in overall accuracy from 81% to 95% (Table 5). NOBS, the most spatially complex site, had the greatest number of classes and, consequently, the lowest accuracy. AGRO, being an intensive agricultural cropland, had the simplest spatial structure and the least number of classes. It also had the highest overall accuracy. At NOBS, the greatest proportion of mapping errors were associated with woody savanna being mapped as savanna (7/68) or evergreen needleleaf forest (11/68) and savanna being mapped as woody savanna

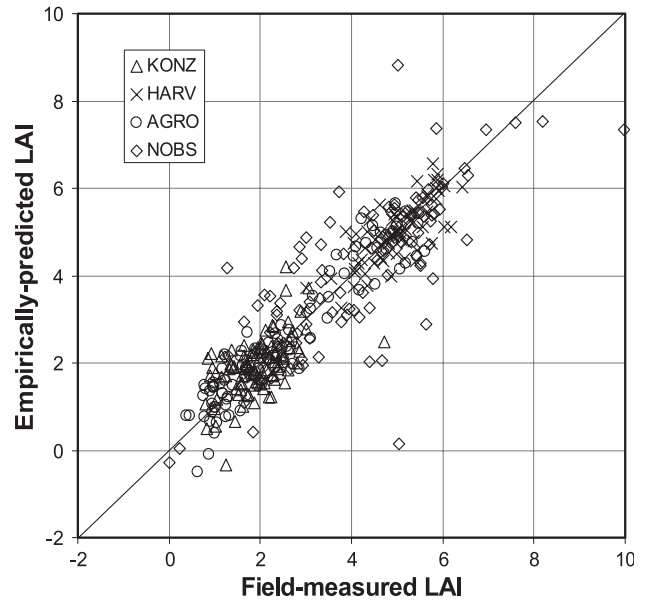


Fig. 5. Cross-validation of BigFoot LAI models/maps.

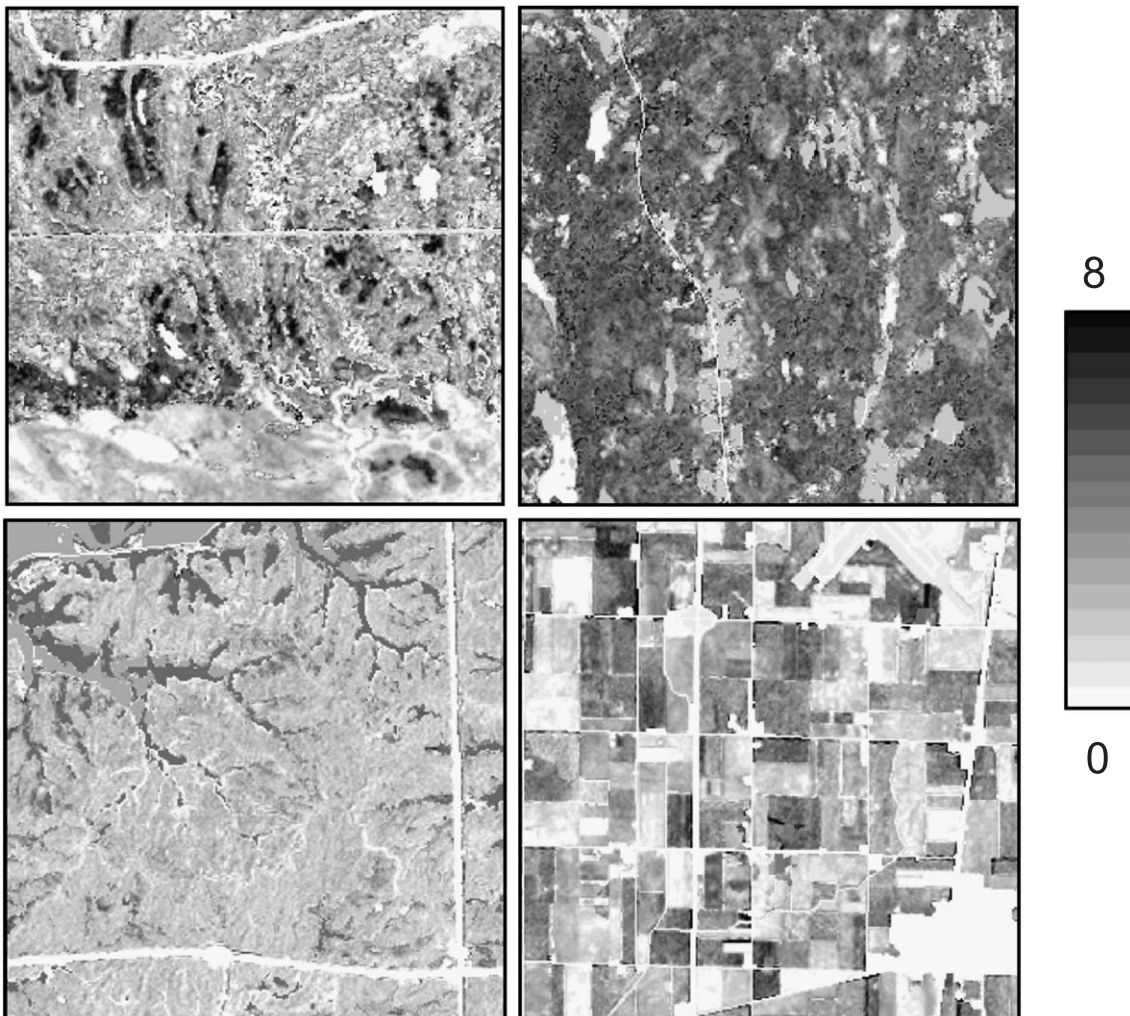


Fig. 4. BigFoot LAI maps based on ETM+ data for the four study sites (upper left, NOBS; upper right, HARV; lower left, KONZ; lower right, AGRO).

Table 6
Cross-validation results for BigFoot 2000 LAI predictions

Site	Correlation coefficient	RMSE	Bias	Variance ratio
NOBS	0.78	1.17	-0.01	1.01
HARV	0.75	0.48	0.00	1.04
KONZ	0.54	0.60	0.00	1.13
AGRO	0.94	0.50	0.00	1.00
All sites	0.90	0.77	0.00	1.01

(8/49). At HARV, the only significant mapping error was deciduous broadleaf forest being mapped as mixed forest (8/60). There was a tendency to map open shrubland as grassland (10/56) at KONZ and for savanna to be mapped as open shrubland (4/6) or woody savanna (2/6). No significant mapping errors occurred at AGRO. In general, cover mapping errors were well balanced.

3.2. BigFoot LAI

At each site, mapped LAI patterns generally followed patterns of land cover across the site (Fig. 4; compare with Fig. 3). Predicted (from cross-validation) versus observed (from field measurements) LAI indicated a high degree of correspondence between field-based measures and remotely sensed predictions of LAI (Fig. 5). This is true both at the site level and across sites (Table 6). In all cases, there was essentially no bias in the predictions and the variance ratio was near 1.0, suggesting preservation of observed variance in the predictions.

3.3. BigFoot–MODIS comparisons: land cover

Direct comparisons of BigFoot (reprojected from Fig. 3) and MODIS (Fig. 6) land cover maps for 2000 revealed several important distinctions and similarities. One obvious

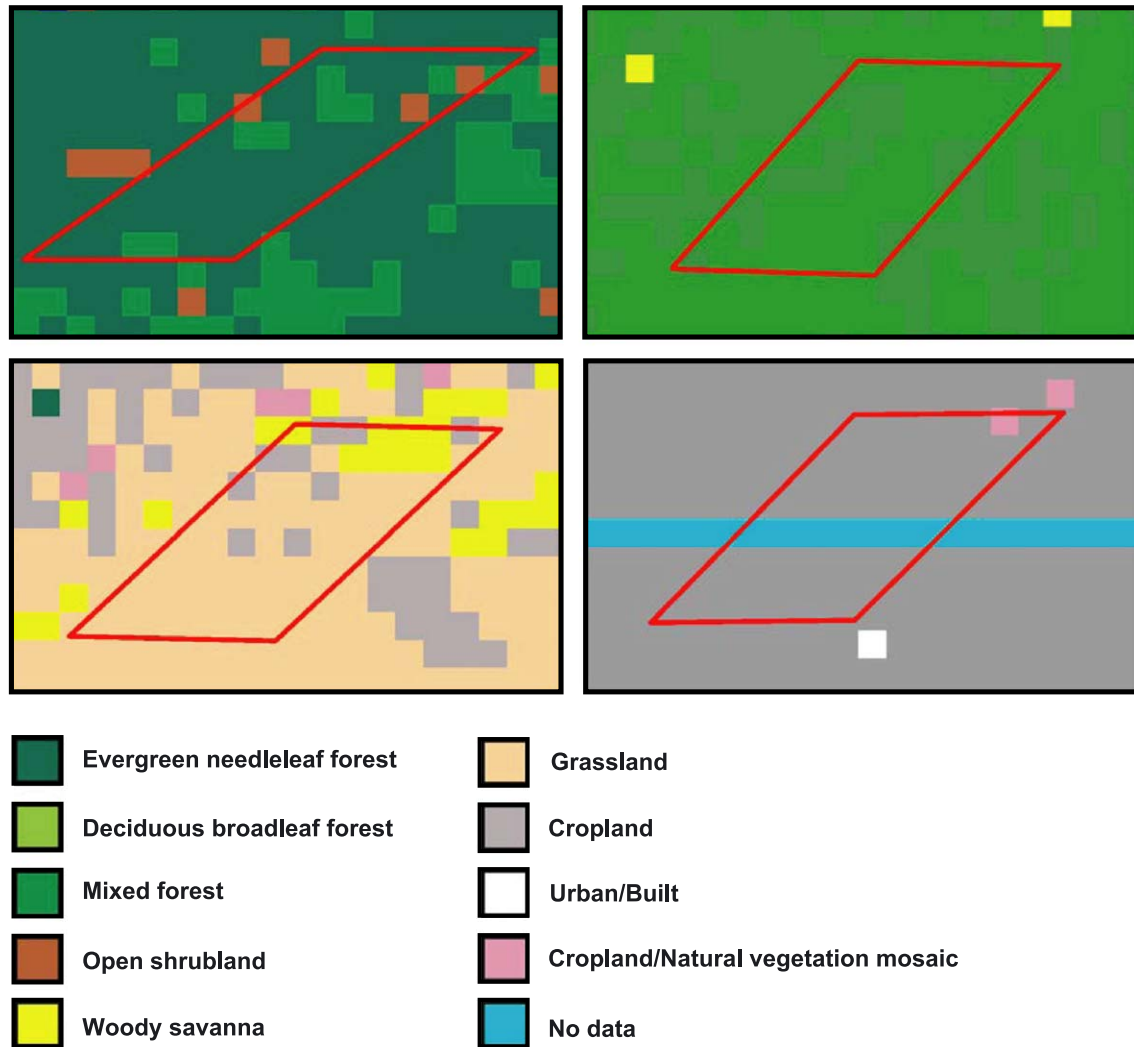


Fig. 6. MODIS land cover maps for the four study sites (upper left, NOBS; upper right, HARV; lower left, KONZ; lower right, AGRO). Also shown are the parallelogram-shaped boxes that define the study sites in ISIN projection.

difference was associated with image/map resolution. BigFoot maps, being based on Landsat ETM+ data, captured much of the spatial complexity of land cover at the sites. In contrast, the relatively coarse resolution of MOD12Q1 did not allow for that level of spatial detail. This difference was most striking at NOBS, the most spatially complex site. However, this observation was relevant at the simplest site, AGRO, where finer detail of individual fields, roads, and water courses was absent. Another difference, specific to NOBS, was an apparent overprediction of tree cover percentage relative to BigFoot. For 2000, MOD12Q1 suggested this site was largely an evergreen needleleaf forest, whereas BigFoot mapped the site largely as open shrubland, woody savanna, and savanna (Fig. 7). There was little change at this site between 2000 and 2001 according to the BigFoot analysis, whereas the MODIS product contained a greater proportion of evergreen needleleaf forest. At HARV, a closed forest system, MOD12Q1 and BigFoot agreed in 2000 over a substantial portion of the landscape that the predominant cover types were deciduous broadleaf and mixed forest. For 2001, the MODIS product contained less mixed forest and more deciduous broadleaf, whereas the BigFoot map indicated the site had not substantively changed. At KONZ, which BigFoot mapped largely as grassland, punctuated by deciduous broadleaf forest and open shrubland in both years, MOD12Q1 also mapped the area largely as grassland both

years. However, MOD12Q1 had more of the area mapped as cropland than did BigFoot, particularly in 2001. There was excellent agreement between the two maps at AGRO, where most of the area was mapped as cropland in 2000.

3.4. BigFoot–MODIS comparisons: LAI

For 2000, BigFoot and MOD15A2 LAI products were not directly compared. However, placing both 2000 and 2001 BigFoot map data on the graphs containing the MOD15A2 LAI trajectories for 2001 (Fig. 8) provided some meaningful insights into the behavior of MOD15A2 Collection 3 provisional products. In 2000/2001, NOBS was a boreal forest ecosystem consisting largely of black spruce forests of varying density (i.e., savanna, woody savanna, and evergreen needleleaf forest). As such, LAI was fairly stable at this site throughout the growing season. That there was such distinct seasonality in the MOD15A2 LAI trajectory for this site in 2001 is likely due to several factors. The most important influence is from changes in surface reflectance: in the winter, ground cover consists largely of snow and ice; these are replaced by extensive moss cover in the summer. Also, during the growing season, MOD15A2 LAI was not stable. Maximum, site-level mean LAI occurred in early July (Day 185, Table 7), at a value of 5.4, but this declined fairly steadily from that

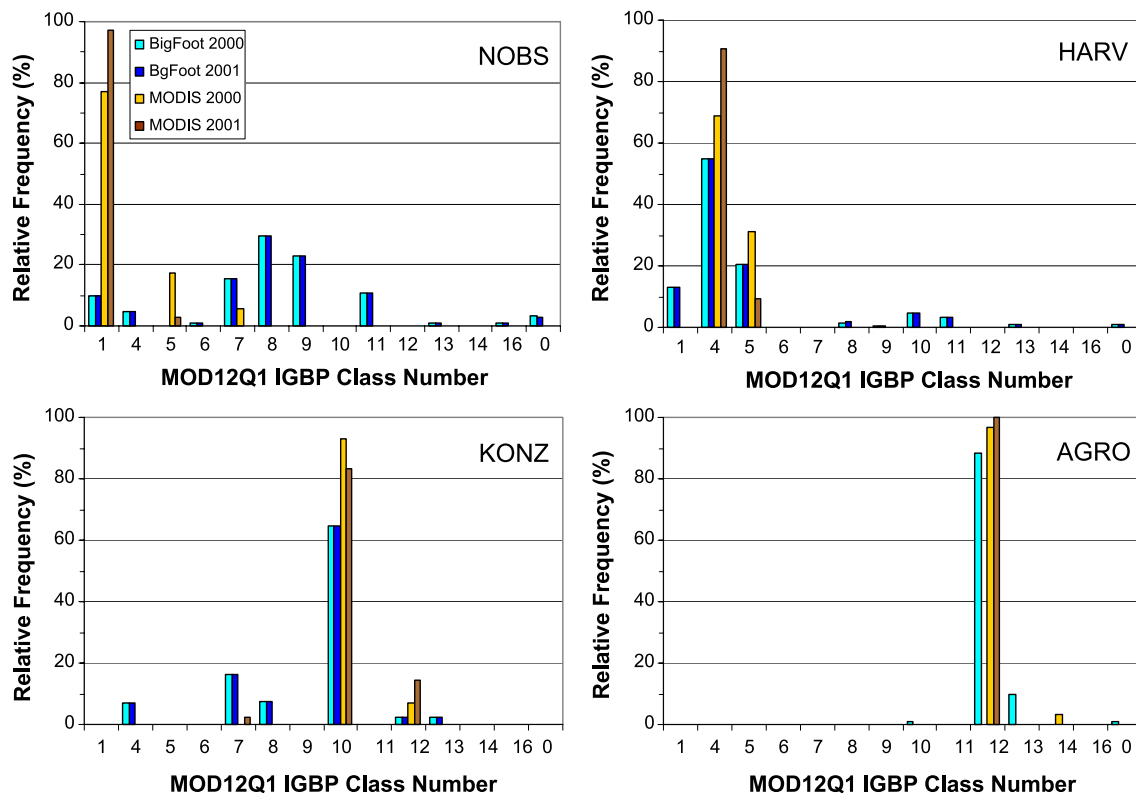


Fig. 7. Relative proportions of land cover types at each site in 2000 and 2001, as mapped by BigFoot (except AGRO 2001) and MODIS. Only those MODIS cells that were completely filled by ETM+ maps over the 7 × 7 km area of each site are included. See Table 2 for class names.

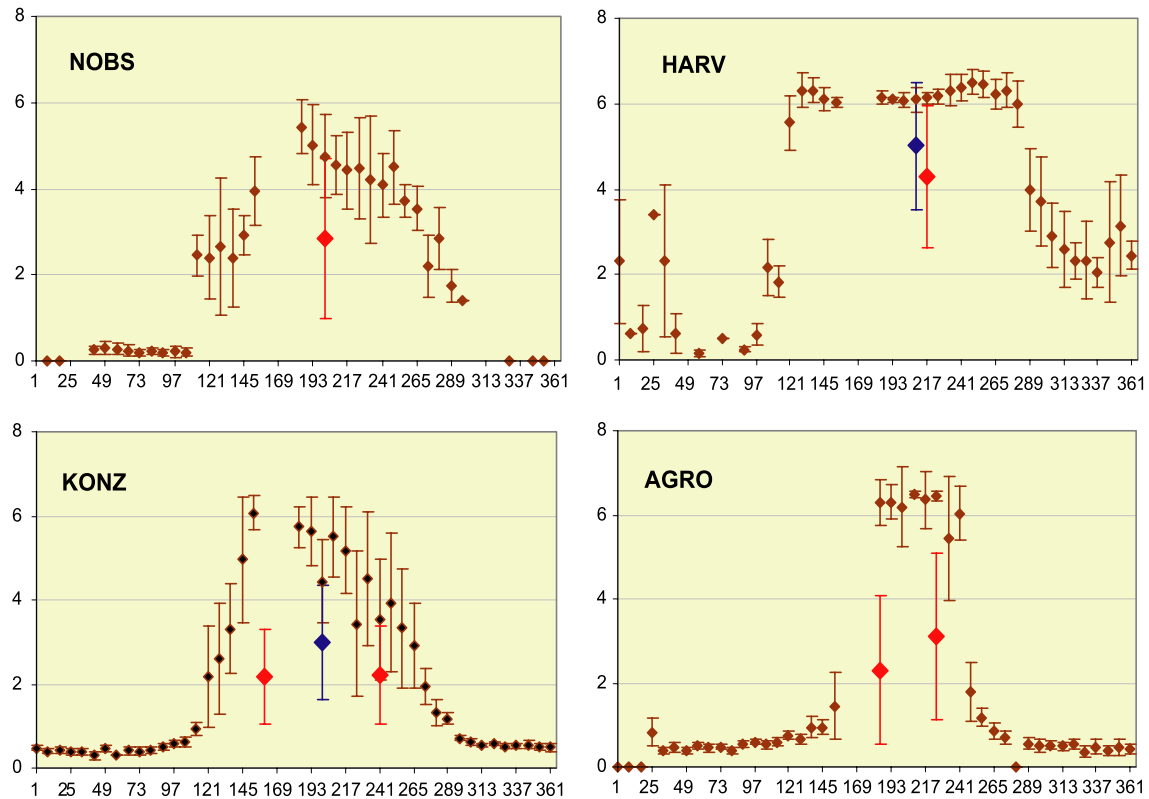


Fig. 8. MODIS 2001 LAI trajectories for each site. Means and one standard deviation are shown in brown. Only those MODIS estimates for Quality Flags 0 and 4 are shown. Missing data are a function of cloudiness and MODIS sensor problems. BigFoot data are in red (2000) and blue (2001). For 2001 at NOBS, data are not shown as they are the same as for 2000. See Table 7 for the date equivalents of the bin numbers shown on the x-axis.

point on. Much of this instability was likely due to sun-angle effects on reflectance at this high-latitude site. BigFoot LAI was estimated from allometric equations, with a mean field-measured value of 4.0 (Table 8). Five percent of NOBS was unvegetated (i.e., water, barren, urban/built) and 10% was mostly nontree wetland (11%) (Fig. 7). As MODIS data contain these areas as well as the more vegetated forest classes, the most directly relevant BigFoot data were the ETM+ LAI products. Across the 7×7 km mapped area coincident with the MODIS products, mean LAI was 2.8 for both 2000 and 2001 (Fig. 8). At HARV, the shape of the seasonal trajectory can largely be explained by vegetation dynamics, as this site was dominated by deciduous broadleaf trees. During the peak of the growing season from May through September, the MODIS product indicated a mean LAI of about 6.1. The field measurements at vegetated plots in 2000 and 2001, respectively, yielded an average LAI of 5.0 and 5.5 (Table 8). Inclusion of nonvegetated areas yielded a mean LAI of 4.3 across the site in 2000 and 4.9 in 2001 (Fig. 8).

Overall, the shapes of the seasonal trajectories of MODIS 2001 at KONZ and AGRO follow expected trajectories for grassland and intensive agriculture (Fig. 8). However, the MODIS product indicated values of between 4.0 and 6.0 during the 2001 growing season at KONZ (Fig. 8), whereas BigFoot field measurements from 2000 indicate

that the vegetated plots had LAI values of 2.0 at KONZ at two separate times during the 2000 growing season and 2.9 during the midpoint of the 2001 growing season (Table 8). With minimal nonvegetated areas at this site, the ETM+ map values and the field-measured values were similar (Fig. 8). At AGRO, MODIS 2001 LAI values were in excess of 6.0 throughout the peak of the growing season. BigFoot 2000 field measurements averaged between 2.5 and 3.6 during the most active growing period. ETM+ maps values were similar to those of the field values at this intensively cropped site. Note that the standard deviations shown in Fig. 8 are always higher for the BigFoot products than for the MODIS products. This is largely due to the grain size differences of the two products.

From the MODIS provisional Collection 4 LAI products we evaluated, it is clear that Collection 4 is different than Collection 3. Most importantly, the Quality Flag definitions are quite different, with “best” retrievals coming from either the main or backup algorithm in Collection 3, whereas in Collection 4, only main algorithm retrievals were labeled as best. Of the 245 possible number of LAI retrievals (5 date-bins \times 49 1-km pixels) per site, Collection 3 data contained as low as 195 (KONZ), and as high as 236 (NOBS), best retrievals, for an average rate of 91% (Table 9). In contrast, Collection 4 best retrievals ranged from 1 (HARV) to 45 (NOBS), with an average retrieval rate of 12%. The mean

Table 7
Date equivalents for bin numbers in Figs. 8 and 9

Bin	Date in 2001
1	1-Jan
9	9-Jan
17	17-Jan
25	25-Jan
33	2-Feb
41	10-Feb
49	18-Feb
57	26-Feb
65	6-Mar
73	14-Mar
81	22-Mar
89	30-Mar
97	7-Apr
105	15-Apr
113	23-Apr
121	1-May
129	9-May
137	17-May
145	25-May
153	2-Jun
161	10-Jun
169	18-Jun
177	26-Jun
185	4-Jul
193	12-Jul
201	20-Jul
209	28-Jul
217	5-Aug
225	13-Aug
233	21-Aug
241	29-Aug
249	6-Sep
257	14-Sep
265	22-Sep
273	30-Sep
281	8-Oct
289	16-Oct
297	24-Oct
305	1-Nov
313	9-Nov
321	17-Nov
329	25-Nov
337	3-Dec
345	11-Dec
353	19-Dec
361	27-Dec

value of the best retrievals from Collection 3 and Collection 4, respectively, for each site, were 5.0 and 4.6 (NOBS), 6.1 and 5.6 (HARV), 5.1 and 2.1 (KONZ), and 6.4 and 2.3 (AGRO).

Of the 223 non-best retrievals for Collection 4 at AGRO, most of these (179) went into the “255 fill” category, which means no prediction was made (Table 9). At NOBS, the 200 non-best retrievals went into nine other flag categories that we labeled as “other” in Table 9. At HARV, the 244 non-best went into 14 other non-best categories, and at KONZ the 199 non-best retrievals went into 8 non-best categories and four pixels went into the 255 fill category. The actual descriptions of the Quality Flags in Collection 4 are not easy

Table 8
Mean and standard deviation of LAI field measurements

Site	Year	Date	Mean	S.D.
NOBS	1999	May–September	4.03	1.75
HARV	2000	June	5.08	0.85
		August	4.99	0.67
	2001	July	5.54	0.81
KONZ	2000	June	1.96	0.62
		August	2.02	0.81
	2001	July	2.90	0.85
AGRO	2000	July	2.47	1.50
		August	3.60	0.87

to understand. For example, Quality Flag 10 is described as not produced due to cloud, clear, and main algorithm with best result.

By site, the mean Collection 4 LAI values for our other category (Table 9) were 4.5 (NOBS), 6.0 (HARV), 2.1 (KONZ), and 3.1 (AGRO). Thus, for Collection 4 at NOBS, there was little difference in mean LAI predictions between best and other retrievals, and the overall prediction difference between Collections 3 (5.0) and 4 (4.6) was small relative to the mean BigFoot ETM+ prediction of 2.8. At HARV, the single best retrieval had a LAI value 0.4 lower than the mean of other retrievals, but the overall prediction difference between Collections 3 and 4 was negligible. At AGRO Collection, four LAIs of the other category averaged 0.8 higher than best, with the average across categories being 2.8. These values are a considerable improvement over the Collection 3 predictions (having a mean in excess of 6), in that they are close to the mean value of approximately 3.0 for the ETM+ predictions at AGRO during the same period. However, 73% of Collection 4 pixels at AGRO consisted of fill values. Finally, at KONZ, there was no difference in the Collection 4 prediction mean between the best and other categories, and the combined mean had a LAI value 0.8 below the mean ETM+ predictions of 2.9 for 2001.

3.5. MODIS reflectance and LAI

The MODIS algorithm has two main pathways: main and backup. The main algorithm is based on radiative transfer

Table 9
Mean LAI values for 245 MODIS predictions evaluated to compare Collections 3 and 4, shown by quality flag group and site

Collection	Quality	Site							
		NOBS		HARV		KONZ		AGRO	
		n	Mean	n	Mean	n	Mean	n	Mean
3	Best	236	5.0	230	6.1	195	5.1	229	6.4
	Other	9	5.3	15	6.1	50	5.0	16	6.1
	255 Fill	0		0		0		0	
4	Best	45	4.6	1	5.6	42	2.1	22	2.3
	Other	200	4.5	244	6.0	199	2.1	44	3.1
	255 Fill	0		0		4		179	

The predictions consist of 5 date-bins by 49 pixels.

theory (Myneni et al., 2002) and the backup algorithm is semiempirical (<http://cybele.bu.edu/modismisr/products/modis/userguide.pdf>). The main algorithm was designed to utilize all reflectance bands of MODIS data, and it has been tested using the red, near-infrared, and blue bands (Myneni et al., 2002), but the functionality of using all bands does not appear to have been fully exploited in Collection 3 (there is no way for us to determine if this remains true for Collection 4). Rather, it appears that Bands 1 (red) and 2 (near-infrared) are used exclusively, with perhaps the addition of Band 3 (blue) (Myneni et al., 2002). Moreover, according to Myneni et al. (2002), the backup algorithm is explicitly designed to utilize only Bands 1 and 2 (i.e., the NDVI). Interestingly, during the 2001 growing season around the neighborhood of each of the four sites, the backup algorithm, and thus the NDVI, was the predominant means used to estimate LAI in Collection 3 (Fig. 9). It is well known that the NDVI saturates, or is asymptotic with respect to LAI at relatively low values of LAI across numerous vegetation types (e.g., Chen & Cihlar, 1996; Turner et al., 1999). With respect to MOD15A2, this is referred to as the “saturation domain” (Myneni et al., 2002). Using the ETM+ data from each BigFoot plot in conjunction with the 2000 field measurements, we see that, in fact, there was essentially no sensitivity of NDVI to LAI across the full range of LAI values at each site (Fig. 10). In contrast, when other bands were used (Table 10), particularly those in the shortwave-infrared region, at NOBS and KONZ, there was a nearly linear spectral response to

changes in LAI across the measured ranges. At HARV, there was only a slightly improved response using the fuller spectral depth of ETM+. It is important to note that the BigFoot LAI maps were not produced using a single spectral relationship with LAI, as shown here, but using class-specific relationships where possible (Table 3; Cohen et al., 2003), which significantly improved the ability to accurately estimate LAI from ETM+.

That ETM+ data exhibit definite linear relationships with LAI does not suggest that MODIS data would likewise exhibit such relationships if greater spectral range than that offered by the NDVI were used. This is because MODIS data have significantly larger grain size (250–1000 m), which can be expected to lower overall spatial variance (Woodcock & Strahler, 1987; Cohen, Spies, & Bradshaw, 1990) and thus, perhaps, spectral sensitivity to LAI regardless of specific spectral ranges used. Furthermore, at larger grain sizes, there is less likelihood that class-specific relationships are practical. Examining MODIS-derived NDVI for the three sites in relation to LAI derived from spatially aggregated, fine-grained BigFoot ETM+ LAI maps, we see that there were again no meaningful relationships (Fig. 10). In contrast, when additional spectral ranges of MODIS data were used, there were still strong, meaningful relationships with LAI at NOBS and KONZ. Moreover, the relationship at HARV was actually improved over that of the finer-grained data. At 1000 m, not only was there still no relationship between MODIS NDVI and LAI, but for all three sites, the strength of relationships actually improved

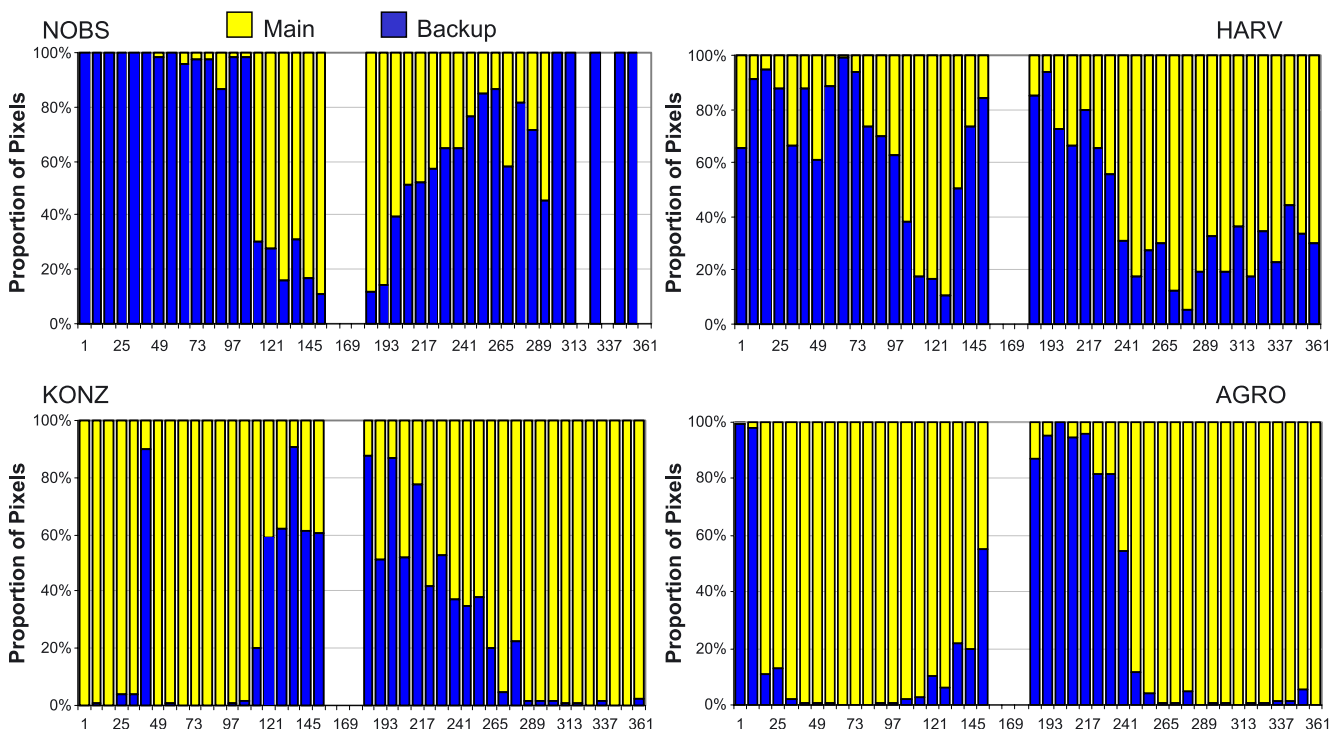


Fig. 9. MODIS LAI algorithm path (main, backup) usage by composite period for 2001 over 10,000 km² surrounding each site. Only those MODIS estimates for Quality Flags 0 and 4 are shown. See Table 7 for the date equivalents of the bin numbers shown on the x-axis.

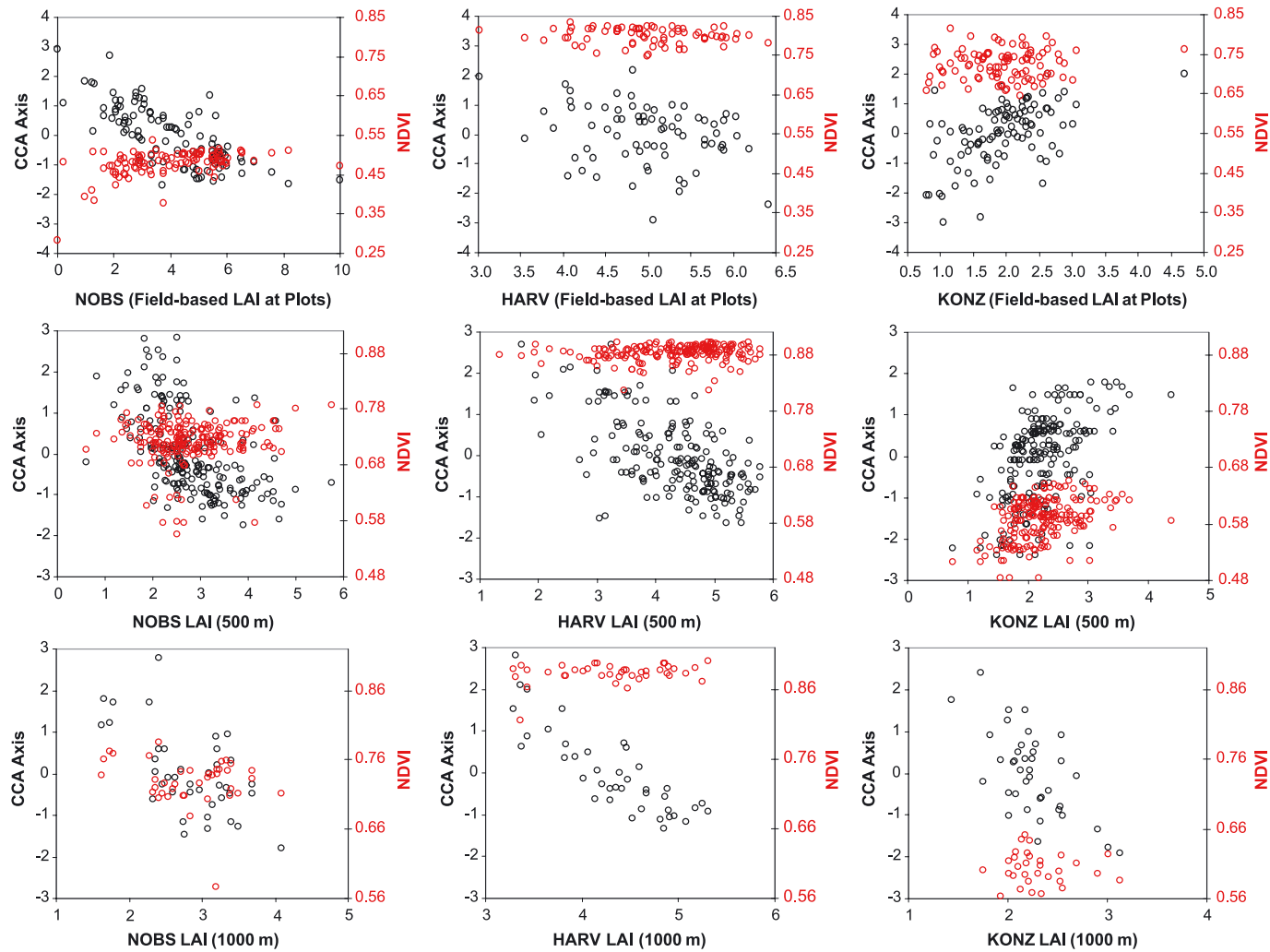


Fig. 10. NDVI and CCA indices as a function of sensor and spatial resolution for NOBS, HARV, and KONZ. Top row is Landsat ETM+ data resampled to 25 m to match field plot size; middle and bottom rows are MODIS data at two spatial resolutions.

Table 10
Correlation coefficients for LAI with ETM+ and MODIS bands, NDVI, and the CCA index

ETM+ band	1	2	3	4	5	7			
Wavelengths (nm)	450–520	520–600	630–690	760–900	1550–1750	2080–2350	NDVI	CCA	
NOBS 25 m	-0.66	-0.62	-0.66	-0.49	-0.64	-0.69	0.45	-0.74	
HARV 25 m	-0.09	0.05	0.00	-0.04	0.03	-0.27	-0.14	-0.27	
KONZ 25 m	-0.13	-0.04	-0.02	0.14	-0.1	-0.29	0.07	0.53	
MODIS band	3	4	1	2	5	6	7		
Wavelengths (nm)	459–479	545–565	620–670	841–876	1230–1250	1628–1652	2105–2155	NDVI	CCA
NOBS 500 m	-0.23	-0.40	-0.36	-0.38	-0.44	-0.48	-0.46	0.10	-0.54
HARV 500 m	-0.49	-0.38	-0.15	-0.01	-0.19	-0.43	-0.44	0.14	-0.63
KONZ 500 m	-0.30	-0.34	-0.41	0.17	-0.09	-0.49	-0.22	0.39	0.52
NOBS 1000 m	-0.20	-0.40	-0.25	-0.54	-0.57	-0.52	-0.51	-0.21	-0.61
HARV 1000 m	-0.74	-0.60	-0.35	-0.18	-0.24	-0.60	-0.65	0.28	-0.85
KONZ 1000 m	-0.24	-0.36	-0.37	0.04	-0.28	-0.50	-0.16	0.32	-0.65

Bold text indicates bands that were included in the CCA index. Bands are listed in order of wavelength range.

over those of the fine-grained and 500-m relationships when more MODIS bands were used. Most noticeable was the improvement at HARV.

Table 10 gives Pearson's product-moment correlation coefficients for the relationships between LAI and reflectance for all ETM+ and MODIS bands used to develop Fig. 10. Correlations varied from an absolute value of zero to 0.74. For the ETM+ data, the most strongly correlated band for all sites was Band 7, in the shortwave-infrared region. For NOBS, all other bands, except Band 4, were nearly equally correlated with LAI as was Band 7. All bands were negatively correlated with LAI, such that the NDVI was less effective than any of the bands individually. The CCA index, which incorporated Bands 1, 5, and 7, was more highly correlated than any of the individual bands. At HARV, both Bands 1 and 7 were included in the CCA index, although the index was no more strongly correlated with LAI than was Band 7. At KONZ, where all bands were included in the CCA index, its correlation with LAI was significantly greater than the correlation with Band 7 alone. For both HARV and KONZ, the NDVI was significantly less correlated with LAI than were both Band 7 and the CCA index.

At 500-m resolution, the three shortwave-infrared bands of MODIS (5, 6, and 7) were the most highly correlated with LAI at NOBS, although all other bands except 3 (in the blue) were nearly equally correlated (Table 10). At HARV, MODIS Bands 6 and 7, along with Band 3, were the most strongly correlated with LAI, whereas at KONZ, Bands 6 and 1 (red) were most highly correlated. At NOBS and HARV, all bands were incorporated into the CCA index, and that index was the most highly correlated spectral variable. The same is true at KONZ, except that only Band 2 (near-infrared) was included with the shortwave-infrared bands in the CCA index. The NDVI was only weakly correlated with LAI at all three sites. At 1000-m resolution, we saw the same general results as at 500 m, with the CCA indices being the most strongly related to LAI and the shortwave-infrared being among the most important spectral bands

contributing to that strength. Again, the NDVI was only weakly correlated to LAI.

4. Discussion and conclusions

4.1. BigFoot approach to validation

Validation of MODIS products related to the terrestrial carbon cycle requires an integrated approach based on field measurements (including those made by flux towers), remote sensing, and models. As MODIS products are global, their validation should also be global. For this, it is useful to stratify the biosphere by major biome type and focus at least one validation effort in each biome. BigFoot is only one of the numerous validation efforts that considers the problem in this way, and for several biomes, there are numerous validation efforts (Morissette et al., 2002). However, not all validation projects will come to the same conclusions about specific MODIS products. This is because of variations in approaches to validation; such things as field sampling design and measurement methods, uniqueness of specific studies sites, types of remote sensing datasets and their analyses, specific types of extrapolation models and conceptual frameworks for integration, and researcher biases are often quite different. The approach taken by BigFoot has been to work over an area at a given site that is large enough to enable validation in terms of multiple MODIS cells (>25), to sample each site with field measurements in a way that captures the ecological variability at each site, to use Landsat ETM+ data to develop accurate surfaces (or maps) of measured variables at a grain size commensurate with the measurements, to drive spatially explicit ecosystem process models that capture carbon dynamics using those ETM+ surfaces, to characterize the errors in the fine-grained surfaces, and then to compare these surfaces with those of a similar thematic content derived by MODIS data and algorithms.

For land cover and LAI, our remote sensing methods were empirical; our goal being to derive surfaces that would extrapolate observations in a way that would achieve relatively high accuracy and that would provide balanced errors. Given the number of land cover classes to map at several of our sites, that we accomplished overall accuracies in excess of 80% (88% across sites) is quite good relative to what can be expected based on the published literature. We attribute this to working over areas on the ground that could be extensively characterized in the field, coupled with simple, but effective statistical approaches and, where needed, hand editing. Many of the IGBP classes are based on percent tree cover, and where in some cases we overestimated tree cover, in others we underestimated cover. For mapping LAI, our desire to balance errors of overprediction with errors of underprediction across observed ranges at each site caused us to explore new approaches to mapping continuous biophysical variables (Cohen et al., 2003). Stratification by major cover type, RMA modeling, and use of multiple spectral variables from multitemporal data series enabled us to predict LAI nearly nonasymptotically across a range of near zero to 10 with an overall 0.90 correlation coefficient of predicted versus observed and low standard errors of estimate.

Having fine-grained maps of land cover and LAI that were well-georeferenced gave us the flexibility to match these maps with MODIS data and products rather precisely, given that MODIS data were also well-georeferenced. This meant that we could do meaningful comparisons (i.e., validation) over the same nearly exact 49-km² areas on the ground. Moreover, by extending our analysis beyond the MODIS LAI product, we were able to use our LAI maps as reference for an examination of MODIS spectral properties in relation to LAI to determine that the MODIS data themselves are well correlated with LAI at spatial resolutions up to 1 km.

4.2. MODIS land cover product quality

MODIS land cover products exist in several variants (Friedl et al., 2002). We choose to validate the IGBP variant, as it is expected to be the most widely used. The IGBP product has 1-km spatial resolution and was generated using an empirical, supervised classification strategy that relies on a global database of training sites that were interpreted for land cover class by examining high-resolution imagery and ancillary data. The training database, STEP (Muchoney, Strahler, Hodges, & LoCastro, 1999), is geographically comprehensive and contained 1373 sites (Friedl et al., 2002) with numerous examples, capturing variation within each land cover class. Most of the land cover interpretations were based on Landsat data and expert knowledge. Inputs to the algorithm include seven MODIS reflectance bands (specifically the NBAR product described by Schaaf et al., 2002) and the EVI product (Huete et al., 2002). The algorithm is designed to be most effective using a full year

of MODIS data. Although this requirement was satisfied for the 2001 product, the 2000 product was based on only one-half year of data. The algorithm itself is a univariate decision tree that incorporates boosting, or voting, which minimizes sensitivity to noise in the spectral data (Friedl et al., 2002). To assess the quality of the product, Friedl et al. use a form of cross-validation that is associated with boosting.

Early results of “in-house” validation suggest that the 2000 provisional product is realistic and that the algorithm performed well at the global scale (Friedl et al., 2002). The quality of the product appears to decrease at increasing latitudes because of missing data and low sun angles and there was excessive confusion between natural and agricultural vegetation throughout. BigFoot results corroborated this assessment. For 2000, the land cover class distributions at HARV, KONZ, and AGRO were quite similar for MODIS and BigFoot products. At NOBS, however, which is a high-latitude site, there was considerable misclassification in the MODIS product. Although the site was mostly classified by MODIS as a “treed” or “forest-like” site, the misclassification was associated with an overprediction of evergreen needleleaf cover, forcing savanna and woody savanna to be classified as “closed canopy” forest. At KONZ and AGRO, the problem with misclassification of agricultural cropland was evident in that there was some overestimation of cropland at these sites. But overall, cropland estimates were similar for the two products.

The MODIS land cover product for 2001 was based on 12 months of data. As such, given the algorithm is designed for ingest of a full year of MODIS data, we would expect improvement in the product. Overall, the results from comparisons with 2001 BigFoot maps were similar to those of comparisons with 2000 BigFoot maps. However, what we saw from our four sites was that the classifications were trending toward more pure conditions. For example, at NOBS, there was more evergreen needleleaf forest in 2001 than in 2000. Similarly, at HARV, whereas there was more mixed forest in 2000, much of that has moved to the deciduous broadleaf class. At AGRO, the site went to 100% cropland, at the expense of the mosaic class. The exception was KONZ, where, although the grassland class decreased to levels closer to those of BigFoot estimates, there was an increase in cropland at this site.

The IGBP classification scheme is not without problems. For example, an ideal classification scheme should have a total set of nonoverlapping classes; that is, the set should be all encompassing and mutually exclusive. Ideally, the classes should also be quantitatively defined. For the forest classes (1 through 5, Table 2), these standards are more or less met. Classes 8 and 9, woody savanna and savanna, respectively, would also appear to meet acceptable quantitative definition standards. These seven classes are all defined in terms of their woody cover components, and all require that the woody vegetation be over 2 m in height. But what of the shrub classes? If an area has, for example, 70%

shrub cover and 20% or 30% tree cover, is it Class 6 (closed shrubland) or Class 9 (savanna)? Likewise, if an area has 20% shrub cover and 40% tree cover, is it Class 7 (open shrubland) or Class 8 (woody savanna)? Other such examples are relatively easy to find using these classes alone. But what of Class 13 (urban/built)? Many urban/suburban areas have extensive tree, shrub, and grass cover, and how does one decide which class to use as a label for such areas? Perhaps the most poorly defined class is number 11, permanent wetland. The basic requirement is for “permanent” water. This literally could encompass all of the classes from 1 through 10, and how much of the total area needs to be in that permanent water condition? Moreover, what about the vast coastal wetland areas that are more influenced by tidal activity, where the “permanence” element is brought into question?

4.3. MODIS LAI product quality

The main MODIS LAI algorithm is designed to ingest up to seven spectral bands and related quality information from MODIS (Myneni et al., 2002). The algorithm outputs for each 1-km cell are the most probable values of LAI from lookup tables (LUTs) developed by iterative runs of a radiative transfer model using expected distributions of various parameters (Knyazikhin et al., 1999; Myneni et al., 2002). The assigned value for a given MODIS cell is the mean of the retrieved distribution. The main algorithm can also ingest multiangle reflectance from the MISR sensor, but appears to be quite sensitive to red and near-infrared reflectance derived from MODIS, as it will fail to retrieve LAI values when MODIS NDVI is higher or lower than expected for a given biome (Myneni et al., 2002). The main algorithm path is designed to be further limited when additional reflectance bands or MISR data are used, such that LUTs incorporating modeled canopy structural properties are included that further constrain the algorithm. When the ingested spectral data fall outside the realm of expected values (i.e., modeled values, and influenced by upstream algorithm errors such as MODIS reflectance calibration) for a given biome, there is no retrieval from the LUTs, and a backup algorithm is used. This backup algorithm is based on a regression relationship between (model-derived) LAI and NDVI values, where a single relationship has been derived for each of six global vegetation types, or biomes (Knyazikhin et al., 1999). More nonretrievals are expected with increasing pixel (or grain) size, as biome mixtures become more common. However, although the algorithm is sensitive to biome misclassification, if the misclassification is of a similar class as the “true” class (e.g., shrubland versus savanna), the sensitivity is low (Myneni et al., 2002). With so few biome classes, the likelihood of misclassification is relatively low, but one could also expect misclassifications to be generally more critical to the algorithm.

When vegetation densities are high, reflectance from the vegetation is said to be in the “saturation domain” (Myneni

et al., 2002). In practice, this means there is less confidence in the output value of the assigned LAI, as there is a wide range of probable LAI values for a given spectral vector. MISR data are expected to reduce the importance of the saturation domain, but it is unclear how often MISR data are used by the algorithm as this information does not appear to be included in the quality control flags (Table 5 in Myneni et al., 2002). Additional uncertainties for an LAI retrieval are associated with uncertainties in input reflectance and in the models used to generate the LUTs. Although surface reflectance uncertainties are quantified (Liang et al., 2002; Vermote, El Saleous, & Justice, 2002), model uncertainties are largely unknown (Myneni et al., 2002). Collection 4 reflectance data use an improved cloud and related shadow detection algorithm, as well as incorporating improved aerosol characterization (http://modis-land.gsfc.nasa.gov/news/iniv_nws_pgs/c4_descrip.asp). As such, the new reflectance product should improve the quality of each retrieval by the Collection 4 LAI product. As the retrievals from Collection 4 data we evaluated generally do have more realistic LAI values than those in Collection 3, improved reflectances do appear to have helped.

All of the four LAI validation examples shown by Myneni et al. (2002) suggest that there is good agreement between MODIS product values and field measurements (as well as those scaled through ETM+ and IKONOS spectral data). Furthermore, the central conclusion of Myneni et al. (2002) using pre-Collection 4 data is that “The presented results indicate expected and satisfactory functionality of the algorithm in the operational mode”. While we do not dispute results that were illustrated in Myneni et al. (2002), the results of the BigFoot study presented in this paper indicate that the conclusion that performance of the algorithm is satisfactory may be an overgeneralization. In Collection 3, we noted a great sensitivity of MODIS LAI values to background reflectance at our high-latitude NOBS site, and a strong seasonality during the active growing season at that site that was probably associated with sun angle. At the nonforested sites, KONZ and AGRO, LAI was apparently overpredicted by values of up to $4 \text{ m}^2 \text{ m}^{-2}$ throughout the growing season. Even at HARV, where results from MODIS and ETM+ were most alike, there was still a difference on average of about $2 \text{ m}^2 \text{ m}^{-2}$.

In Collection 4, there does in fact appear to be higher quality retrievals, particularly at KONZ and AGRO where LAI retrievals are now very close to what BigFoot measured in the field and mapped through ETM+. However, as noted earlier, the number of best retrievals is significantly lower in Collection 4, and for AGRO most of the MODIS pixels had fill values. At NOBS, there was essentially no LAI difference in the retrievals between Collections 3 and 4, with both remaining significantly higher than BigFoot ETM+ estimates. At HARV, there also was a negligible difference in retrieval values. As such, the only major improvement we noted between Collections 3 and 4 was at KONZ, where, rather than

having mean LAI values in excess of 2 relative to ETM+ values, Collection 4 means represented an underprediction of 0.8.

BigFoot sites, at 49 km², are not large. One obvious question might be: Do these results hold over larger areas? As a simple test of this, we constructed graphs similar to those of Fig. 8, but containing Collection 3 LAI trajectories for 10,000-km² areas centered on the BigFoot sites. The resulting trajectories were nearly identical to those of the ones based on 49 km² except for a slightly greater variability of values at each composite period. The large majority of MODIS LAI values for 10,000 km² areas centered on the BigFoot sites throughout the growing season at each site were from the backup NDVI-based algorithm (Fig. 9). It is important to note here that when we stratified these large-area predictions on the basis of main versus backup algorithm use, the differences in the prediction values were small (0.6 at NOBS, -0.1 at HARV, 1.0 at KONZ, and 0.6 at AGRO, with positive values indicating higher predictions for the backup algorithm).

There may be numerous reasons why, for Collection 3, the main algorithm did not function as expected over the regions around our study sites. Certainly, the algorithm's sensitivity to reflectance calibration is an important issue, but with Collection 4, that problem should be less important. Also, with Collection 4, the improved MODIS land cover product is being used, which should minimize misclassification impact on the main algorithm. However, given the low rate of LAI retrievals by the main algorithm in Collection 4 data, problems remain. As we demonstrate in this paper, one potentially important improvement would be active incorporation of more MODIS bands into the retrieval process, particularly shortwave-infrared bands.

One rather surprising result from this study is the definite and increasing sensitivity of spectral indices as one moves from ETM+ grain size to 1-km MODIS grain size across multiple biome types. However, this is clearly only the case if spectral bands outside the NDVI range are included, particularly those in the shortwave-infrared.

4.4. Future steps for MODIS validation by BigFoot

The BigFoot project continues its work at the four sites described here. From current and future analyses, we will be able to characterize trends in the MODIS products in relation to what we understand to be happening at the site level from field visits and associated measurements, remote sensing with ETM+, and modeling exercises. Our work will include an evaluation of MOD17 products (i.e., gross primary production, net photosynthesis, and net primary production) and of the fAPAR (or FPAR, as it is otherwise known) component of MOD15A2. We also have begun our work at five additional sites: Arctic tundra, desert grassland, tropical broadleaf forest, dry temperate needleleaf forest, and an additional temperate mixed forest (similar to HARV).

The original sample design for BigFoot fieldwork (Burrows et al., 2002) was an excellent starting point for the project, as we had no good, known way to determine the spatial properties of the variables of interest at each of our landscapes. Having been through the full set of field measurements and remote sensing at each site at least once, we have learned that the ETM+ data are very informative with respect to those spatial properties. As a result, we now have a new design for selection of plots for field measurements that takes better advantage of spectral data to insure sampling of nearly full distributions of vegetation conditions at each site. This will be described in an upcoming paper.

Acknowledgements

This research was funded by NASA's Terrestrial Ecology Program. We greatly thank Robert Kennedy for his contributions to the project, and to all of those who helped collect the field data, including Al Kirschbaum, John Lennon Campbell, Drew Feldkirschner, and Sean Burrows. We owe much appreciation to Jeff Morissette and Jaime Nickeson for their help in so effectively coordinating MODIS validation activities, and to several people on the various MODIS science teams who are too numerous to list here. Thanks to Ramakrishna Nemani and three anonymous reviewers for their extremely helpful and constructive comments on the manuscript.

References

- Baldocchi, D., Falge, E., Gu, L., Olson, R., Hollinger, D., Running, S., Anthoni, P., Bernhofer, C., Davis, K., Evans, R., Fuentes, J. D., Goldstein, A. H., Katul, G., Law, B. E., Lee, X., Malhi, Y., Meyers, T., Munger, J. W., Oechel, W., Paw, K. T., Pilegaard, K., Schmid, H. P., & Valentini, R. (2001). Fluxnet: A new tool to study the temporal and spatial variability of ecosystem-scale carbon dioxide, water vapor and energy flux densities. *Bulletin of the American Meteorological Society*, 82, 2415–2434.
- Berterretche, M., Cohen, W. B., Hudak, A. T., & Gower, S. T. (in review). Comparison of regression and geostatistical methods to develop remote sensing-based LAI surfaces for NPP modeling. *Remote Sensing of Environment*.
- Burrows, S., Gower, S., Clayton, M., Mackay, D., Ahl, D., Norman, J., & Diak, G. (2002). Application of geostatistics to characterize leaf area index (LAI) from flux tower to landscape scales using a cyclic sampling design. *Ecosystems*, 5, 667–679.
- Burrows, S. N., Gower, S. T., Kirschbaum, A. A., Feldkirschner, D. C., Campbell, J. L., Cohen, W. B., Turner, D. P., & Running, S. W. (in review). Geostatistical estimation of leaf area index to validate MODIS products in four North American biomes. *Landscape Ecology*.
- Butera, M. K. (1986). A correlation and regression analysis of percent canopy closure versus TMS spectral response for selected forest site in the San Juan National Forest, Colorado. *IEEE Transactions on Geoscience and Remote Sensing*, 24, 122–129.
- Campbell, J. L., Burrows, S., Gower, S. T., & Cohen, W. B. (1999). BigFoot: Characterizing land cover, LAI, and NPP at the landscape scale for EOS/MODIS validation. *Field manual 2.1. Environmental Science Division Pub. No. 4937*. Oak Ridge, TN: Oak Ridge National Laboratory.

- Chavez Jr., P. (1996). Image-based atmospheric corrections—revised and improved. *Photogrammetric Engineering and Remote Sensing*, 62, 1025–1036.
- Chen, J. M., & Cihlar, J. (1996). Retrieving leaf area index of boreal conifer forests using Landsat TM images. *Remote Sensing of Environment*, 55, 153–162.
- Cohen, W. B., & Justice, C. (1999). Validating MODIS terrestrial ecology products: Linking in situ and satellite measurements. *Remote Sensing of Environment*, 70, 1–3.
- Cohen, W. B., Maierpserger, T. K., Gower, S. T., & Turner, D. P. (2003). An improved strategy for regression of biophysical variables and Landsat ETM+ data. *Remote Sensing of Environment*, 84, 561–571.
- Cohen, W., Spies, T., & Bradshaw, G. (1990). Semivariograms of digital imagery for analysis of conifer canopy structure. *Remote Sensing of Environment*, 34, 167–178.
- Cressie, N. (1991). *Statistics for spatial data*. New York: Wiley.
- Crist, E. P. (1985). A TM tasseled cap equivalent transformation for reflectance factor data. *Remote Sensing of Environment*, 17, 301–306.
- Crist, E. P., & Cicone, R. C. (1984). A physically-based transformation of thematic mapper data—The TM tasseled cap. *IEEE Transactions on Geoscience and Remote Sensing*, GE-22, 256–263.
- Curran, P. J., & Hay, A. (1986). The importance of measurement error for certain procedures in remote sensing at optical wavelengths. *Photogrammetric Engineering and Remote Sensing*, 52, 229–241.
- Efron, B., & Gong, G. (1983). A leisurely look at the bootstrap, the jack-knife, and cross-validation. *The American Statistician*, 37, 36–48.
- Fassnacht, K., Gower, S., MacKenzie, M., Nordheim, E., & Lillesand, T. (1997). Estimating the leaf area index of north central Wisconsin forests using the Landsat Thematic Mapper. *Remote Sensing of Environment*, 61, 229–245.
- Friedl, M., McIver, D., Hodges, J., Zhang, X., Muchoney, D., Strahler, A. H., Woodcock, C. E., Gopal, S., Schneider, A., Cooper, A., Baccini, A., Gao, F., & Schaaf, C. (2002). Global land cover mapping from MODIS: Algorithms and early results. *Remote Sensing of Environment*, 83, 287–302.
- Gower, S., Kucharik, C., & Norman, J. (1999). Direct and indirect estimation of leaf area index, fAPAR, and net primary production of terrestrial ecosystems. *Remote Sensing of Environment*, 70, 29–51.
- Huete, A., Didan, K., Miura, T., Rodriguez, E., Gao, X., & Ferreira, L. (2002). Overview of radiometric and biophysical performance of the MODIS vegetation indices. *Remote Sensing of Environment*, 83, 195–213.
- Huete, A. R., Jackson, R. D., & Post, D. F. (1985). Spectral response of a plant canopy with different soil backgrounds. *Remote Sensing of Environment*, 17, 37–53.
- IPCC (2001). Climate change 2001: Synthesis report. In R. T. Watson, & Core Writing Team (Eds.), *A contribution of working groups I, II, and III to the Third Assessment Report of the Intergovernmental Panel on Climate Change*. Cambridge, UK: Cambridge Univ. Press (398 pp.).
- Justice, C., Townshend, J., Vermote, E., Masouka, E., Wolfe, R., Saleous, N., Roy, D., & Morisette, J. (2002). An overview of MODIS Land data processing and product status. *Remote Sensing of Environment*, 83, 3–15.
- Knyazikhin, Y., Glassy, J., Privette, J. L., Tian, Y., Lotsch, A., Zhang, Y., Wang, Y., Morisette, J. T., Votava, P., Myneni, R. B., Nemani, R. R., Running, S. W. (1999). *MODIS Leaf Area Index (LAI) and Fraction of Photosynthetically Active Radiation Absorbed by Vegetation (FPAR) Product (MOD15) Algorithm Theoretical Basis Document*. http://modis.gsfc.nasa.gov/data/atbd/atbd_mod15.pdf.
- Liang, S., Fang, H., Chen, M., Shuey, C., Walthall, C., Dougherty, C., Morisette, J., Schaaf, C., & Strahler, A. (2002). Validating MODIS land surface reflectance and albedo products: Methods and preliminary results. *Remote Sensing of Environment*, 83, 149–162.
- Morisette, J., Privette, J., & Justice, C. (2002). A framework for the validation of MODIS Land products. *Remote Sensing of Environment*, 83, 77–96.
- Muchoney, D., Strahler, A., Hodges, J., & LoCastro, J. (1999). The IGBP DISCOVER confidence sites and the system for terrestrial ecosystem parameterization: Tools for validating global land-cover data. *Photogrammetric Engineering and Remote Sensing*, 65, 1061–1067.
- Myneni, R.B., Hoffman, S., Knyazikhin, Y., Privette, J. L., Glassy, J., Tian, Y., Wang, Y., Song, X., Zhang, Y., Smith, G. R., Lotsch, A., Friedl, M., Morisette, J. T., Votava, P., Nemani, R. R., & Running, S. W. (2002). Global products of vegetation leaf area and fraction absorbed PAR from one year of MODIS data. *Remote Sensing of Environment*, 83, 214–231.
- NRC [National Research Council] (1999). *Our common journey—a transition toward sustainability*. Washington, DC: National Academy Press (363 pp.).
- Oetter, D., Cohen, W., Berterretche, M., Maierpserger, T., & Kennedy, R. (2001). Land cover mapping in an agricultural setting using multiseasonal Thematic Mapper data. *Remote Sensing of Environment*, 76, 139–155.
- Running, S., Baldocchi, D., Turner, D., Gower, S., Bakwin, P., & Hibbard, K. (1999). A global terrestrial monitoring network integrating tower fluxes, flask sampling, ecosystem modeling and EOS data. *Remote Sensing of Environment*, 70, 108–127.
- Schaaf, C. B., Gao, F., Strahler, A. H., Lucht, W., Xiaowen, L., Tsang, T., Strugnell, N. C., Zhang, X., Jin, Y., Muller, J., Lewis, P., Barnsley, M., Hobson, P., Disney, M., Roberts, G., Dunderdale, J. L., Doll, C., d'Entremont, R. P., Hu, B., Liang, S., Privette, J. L., & Roy, D. (2002). First operational BRDF, albedo nadir reflectance products from MODIS. *Remote Sensing of Environment*, 83, 135–148.
- Sellers, P. J. (1987). Canopy reflectance, photosynthesis, and transpiration: II. The role of biophysics in the linearity of their interdependence. *Remote Sensing of Environment*, 21, 143–183.
- Sellers, P., Hall, F., Asrar, G., Strebel, D., & Murphy, R. (1992). An overview of the first international satellite land surface climatology project (ISLSCP) field experiment (FIFE). *Journal of Geophysical Research*, 97(D17), 18345–18371.
- Sellers, P. J., Hall, F. G., Kelley, R. D., Black, A., Baldocchi, D., Berry, J., Ryan, M., Ranson, K. J., Crill, P. M., Lettenmaier, D. L., Margolis, H., Cihlar, J., Newcomer, J., Fitzjarrald, D., Jarvis, P. G., Gower, S. T., Halliwell, D., Williams, D., Goodison, B., Wickland, D. E., & Guertin, F. E. (1997). BOREAS in 1997: Experiment overview, scientific results, and future directions. *Journal of Geophysical Research*, 102(D24), 28731–28769.
- Seong, J., Mulcahy, K., & Usery, E. (2002). The sinusoidal projection: A new importance in relation to global image data. *Professional Geographer*, 54, 218–225.
- Smith, M. O., Ustin, S. L., Adams, J. B., & Gillespie, A. R. (1990). Vegetation in deserts: I. A regional measure of abundance from multispectral images. *Remote Sensing of Environment*, 31, 1–26.
- Song, C., Woodcock, C., Seto, K., Pax Lenney, M., & Macomber, S. (2001). Classification and change detection using Landsat TM data: When and how to correct atmospheric effects? *Remote Sensing of Environment*, 75, 230–244.
- Teillet, P., Barker, J., Markham, B., Irish, R., Fedosejevs, G., & Storey, J. (2001). Radiometric cross-calibration of the Landsat-7 ETM+ and Landsat-5 TM sensors based on tandem data sets. *Remote Sensing of Environment*, 78, 39–54.
- Townshend, J., & Justice, C. (2002). Towards operational monitoring of terrestrial systems by moderate-resolution remote sensing. *Remote Sensing of Environment*, 83, 351–359.
- Tucker, C. J. (1979). Red and photographic infrared linear combinations for monitoring vegetation. *Remote Sensing of Environment*, 8, 127–150.
- Turner, D., Cohen, W., Kennedy, R., Fassnacht, K., & Briggs, J. (1999). Relationships between leaf area index and Landsat TM spectral vegetation indices across three temperate zone sites. *Remote Sensing of Environment*, 70, 52–68.
- Vermote, E., & Justice, C. (2002). Atmospheric correction of MODIS data in the visible to middle infrared: First results. *Remote Sensing of Environment*, 83, 97–111.

- Vogelmann, J., Helder, D., Morfitt, R., Choate, M., Merchant, J., & Bulley, H. (2001). Effects of Landsat 5 Thematic Mapper and Landsat 7 enhanced thematic mapper plus radiometric and geometric calibrations and corrections on landscape characterizations. *Remote Sensing of Environment*, 78, 55–70.
- Wilson, E. O., & Peter, F. M. (Eds.) (1988). *Biodiversity*. Washington, DC: National Academy Press (521 pp.).
- Wolfe, R., Nishihama, M., Fleig, A., Kuyper, J., Roy, D., Storey, J., & Patt, F. (2002). Achieving sub-pixel geolocation accuracy in support of MODIS land science. *Remote Sensing of Environment*, 83, 31–49.
- Woodcock, C. E., & Strahler, A. H. (1987). The factor of scale in remote sensing. *Remote Sensing of Environment*, 21, 311–332.